

Gene Expression Profile in Frontal Cortex in Sporadic Frontotemporal Lobar Degeneration-TDP

Pol Andrés-Benito, MSc, Ellen Gelpi, MD, PhD, Mónica Povedano, MD, Gabriel Santpere, PhD, and Isidro Ferrer, MD, PhD

Abstract

Molecular alterations compromising key metabolic pathways are poorly understood in sporadic frontotemporal lobar degeneration with TDP-43 pathology (sFTLD-TDP). Whole-transcriptome array, RT-qPCR validation, gel electrophoresis, and Western blotting, and mitochondrial electron transport chain (ETC) activity were comparatively examined in frontal cortex (area 8) of 16 sFTLD-TDP cases and 14 controls. Assessment of 111 genes by RT-qPCR showed downregulation of 81 genes linked to neurotransmission and synapses, neuronal architecture, cytoskeleton of axons and dendrites, vesicle trafficking, purines, mitochondria, and energy metabolism in sFTLD-TDP. Western blotting studies disclosed downregulation of several mitochondrial subunits encoded by genomic DNA and MT-CO1 encoded by the mitochondrial DNA. Mitochondrial ETC activity of complexes I, IV, and V was decreased in sFTLD-TDP. These findings provide robust information about downregulation of genes involved in vital biochemical pathways and in synaptic

neurotransmission which may help to increase understanding about the biochemical substrates of clinical manifestations in sFTLD-TDP.

Key Words: Energy metabolism, Frontotemporal lobar degeneration, Mitochondria, Neurotransmission, Purines, Synapses, TDP43.

INTRODUCTION

Frontotemporal dementia is a progressive neurological disorder characterized by deterioration of personality, behavior, language, and cognition, with marked individual variations, and in the majority of patients is due to frontotemporal lobar degeneration (FTLD). This term stresses the progressive loss of neurons in the frontal and temporal lobes as the cause of the principal neurological symptoms. FTLD is not a unique disease but covers several unrelated conditions: 1) FTLD-tau is identified by the abnormal tau deposition in neurons and glial cells, which in turn encompasses sporadic and genetic forms associated with mutations in *MAPT*, the gene coding for protein tau; and 2) FTLD-U, which is characterized by the presence of intraneuronal ubiquitin-immunoreactive inclusions. Subsequent studies have demonstrated the heterogeneity of FTLD-U, including FTLD-TDP-43 proteinopathy, FTLD-FUS proteinopathy, and FTLD-UPS, lacking TDP-43 and FUS inclusions (1–3).

FTLD-TDP-43 proteinopathy (FTLD-TDP) is clinically manifested by behavioral-dysexecutive disorder, primary progressive aphasia and/or motor disorders including motor neuron disease; macroscopically, by frontal and temporal atrophy, commonly symmetrical, variable involvement of the basal ganglia and substantia nigra; and microscopically, by neuron loss in the cerebral cortex, microvacuolation in the upper cortical layers, astrogliosis, and TDP-43-immunoreactive inclusions in the nucleus and/or cytoplasm of neurons and oligodendrocytes, and in neuropil threads (1–3). Some cases are sporadic (sFTLD-TDP) whereas other are genetic, often familial (fFTLD-TDP) and linked to mutations in different genes including *GRN* (progranulin), *C9ORF72* (chromosome 9 open reading frame 72), *TARDP* (TAR DNA-binding protein), *VCP* (valosin-containing protein), *CHMBP2* (charged multivesicular body protein 2), and *UBQLN* (ubiquilin 2), among others (4–6). Excepting progranulin, mutations of any of the other genes may also be causative of amyotrophic lateral sclerosis (ALS), thus suggesting ALS/FTLD-TDP within the same

From the Neuropathology, Pathologic Anatomy Service, Bellvitge University Hospital, IDIBELL, Hospitalet de Llobregat, Spain (PA-B, IF); Biomedical Network Research Center on Neurodegenerative Diseases (CIBERNED), Institute Carlos III, Hospitalet de Llobregat, Spain (PA-B, IF); Neurological Tissue Bank of the Biobanc-Hospital Clínic-Institut d'Investigacions Biomèdiques August Pi I Sunyer (IDIBAPS), Barcelona, Spain (EG); Institute of Neurology, Medical University of Vienna, Vienna, Austria (EG); Functional Unit of Amyotrophic Lateral Sclerosis (UFELA), Service of Neurology, Bellvitge University Hospital, Hospitalet de Llobregat, Spain (MP); Department of Neurobiology, Yale School of Medicine, New Haven, Connecticut (GS); Department of Experimental and Health Sciences, IBE, Institute of Evolutionary Biology, Universitat Pompeu Fabra-CSIC, Barcelona, Spain (GS); Department of Pathology and Experimental Therapeutics, University of Barcelona, Hospitalet de Llobregat, Spain (IF); and Institute of Neurosciences, University of Barcelona, Barcelona, Spain (IF).

Send correspondence to: Isidro Ferrer, MD, PhD, Department of Pathology and Experimental Therapeutics, University of Barcelona, Campus Bellvitge, c/Feixa Llarga sn, 08907 Hospitalet de Llobregat, Spain; E-mail: 8082ifa@gmail.com

This study was supported by grants from CIBERNED and PI17/00809 Institute of Health Carlos III, and cofunded by FEDER funds/European Regional Development Fund (ERDF)—a way to build Europe; ALS intra-CIBERNED project to IF; and IF115/00035 fellowship to PA-B; grant “Retos todos unidos contra la ELA” to MP; and grant from the “Fundación Tatiana Pérez de Guzmán el Bueno, convocatoria Neurociencias 2014” to EG.

The authors have no competing interests to declare.

disease spectrum (7–9). The presence of TDP-43 inclusions in ALS together with the characteristics of TDP-43, which is phosphorylated, ubiquitinated, and truncated at the C-terminal in both conditions (10), argues in favor of these bounds.

FTLD-TDP has been subclassified into 4 different neuropathologic subgroups that roughly correlate with certain clinical symptoms and genetic substrates although with low predictive value (11, 12). Type A is characterized by numerous neuronal cytoplasmic inclusions (NCIs) and dystrophic neurites (DNs), and variable number of neuronal nuclear inclusions (NIIs) predominating in the upper cortical layers. Type B is delineated by numerous NCIs in the upper and inner cortical layers, and low numbers of DN and NIIs. Type C is defined by predominant DN in the upper cortical layers and rare NCIs and NIIs. Type D is characterized by predominance of NIIs, and rare NCIs and DN (1, 11, 12).

The study of human brain tissue has been useful to unveil additional molecular alterations in FTLT-TDP (13). Complementary information has been obtained using proteomics and transcriptomics in a limited number of FTLT-TDP subtypes including those linked with *GRN* and *C9orf72* mutations, and atypical FTLT-TDP cases (14–17). Gene expression profile has also been recently described in the frontal cortex area 8 in ALS (18) and in different brain regions in sporadic ALS and ALS linked to *C9orf72* mutations (19). However, the molecular pathology of metabolic pathways, mitochondria and energy metabolism, synapses, and neurotransmission has not been studied in sFTLD-TDP. The present study was aimed at analyzing gene expression in frontal cortex area 8 in a series of sFTLD-TDP in parallel with controls in order to gain understanding about vulnerable pathways which can explain pathogenic aspects of the disease.

MATERIALS AND METHODS

Human Cases

Brain samples were obtained from the Brain Banks of the Institute of Neuropathology HUB-ICO-IDIBELL Biobank and the Hospital Clinic-IDIBAPS Biobank following the guidelines of the Spanish legislation on this matter and the approval of the local ethics committees. The postmortem interval between death and tissue processing was between 2 and 18 hours. One hemisphere was immediately cut into 1-cm-thick coronal sections, and selected brain areas were rapidly dissected, frozen on metal plates over dry ice, placed in individual air-tight plastic bags and stored at -80°C until use. The other hemisphere was fixed by immersion in 4% buffered formalin for 3 weeks. The neuropathological study in control and FTLT-TDP cases was carried out on 20 selected 4- μm -thick dewaxed paraffin sections of representative regions of the frontal, temporal, parietal, motor, primary visual, anterior cingulate and entorhinal cortices, hippocampus, amygdala, basal forebrain, caudate, putamen, globus pallidus, thalamus, mid-brain, pons, medulla oblongata, cerebellar vermis, hilus, and cerebral white matter. These were stained with hematoxylin and eosin, Klüber-Barrera, or processed for immunohistochemistry for microglia (Iba-1, Wako, Richmond, VA), glial acidic protein ([GFAP], Dako, Gostrup, Denmark), β -amyloid

(Dako, clone 6F/3D), phospho-tau (Thermo Scientific, Rockford, IL, clone AT8), α -synuclein (Novocastra, Newcastle, UK, clone KM51), TDP-43 (Abnova, Taipei, Taiwan, clone 2E2-D3), ubiquitin (Dako, Polyclonal Rabbit), and p62 (BD Biosciences, San Jose, Purified Mouse Anti-p62 LCK ligand) using EnVision+ System peroxidase (Dako), and diaminobenzidine and H_2O_2 . FTLT-TDP was diagnosed following well-established criteria: frontotemporal atrophy, loss of neurons and variable spongiosis in the upper cortical layers, astrocytic gliosis, and presence of TDP-43-immunoreactive inclusions in neurons and dendrites (NCIs, NIIs, and DN) (1, 11). The whole series included 16 sporadic cases of FTLT-TDP (71.6 ± 9.6 years; 11 men and 3 women), and 14 control cases (66.5 ± 8.8 years; 8 men and 6 women). The postmortem delay varied from 2 hours and 15 minutes to 18 hours ($\sim 5.4 \pm 4.0$) in the control group, and between 3 hours and 40 minutes and 16 hours ($\sim 7.5 \pm 3.9$) in the sFTLD-TDP group. Patients with associated pathologies of the nervous system, excepting early stages of neurofibrillary tangle pathology and mild small blood vessel disease, were not included. Age-matched control cases had not suffered from neurologic and psychiatric disorders and did not show alterations other than those permitted in diseased cases. Regarding TDP types: 11 cases were categorized as type A, 1 as type B, and 4 as type C. A summary of cases is shown in Table 1.

Biochemical studies were carried out in fresh-frozen frontal cortex area 8. Special care was taken to assess pre-mortem and postmortem factors that might interfere with RNA processing and protein integrity (20). For this reason, all the samples were used in the study of RNA expression because RNA integrity values were suitable for RNA study, whereas 10 samples per group were used for gel electrophoresis and Western blotting of samples showing a preserved band pattern after Coomassie Blue staining. The same 10 cases per group were used in the study of mitochondrial enzymatic activities. Cases excluded were neoplastic diseases affecting the nervous system, metabolic syndrome, hypoxia, and prolonged agonic state (such as those occurring in intensive care units), as well as cases with infectious, inflammatory, and autoimmune diseases, either systemic or limited to the nervous system. Assessed samples did not bear *C9ORF72* mutations (21). No other FTLT-TDP-related genes were systematically analyzed.

RNA Purification

RNA from frozen frontal cortex area 8 was extracted following the instructions of the supplier (RNeasy Mini Kit, Qiagen, Hilden, Germany). RNA integrity and 28S/18S ratios were determined with the Agilent Bioanalyzer (Agilent Technologies, Inc., Santa Clara, CA). RNA integrity values are shown in Table 1. Samples were treated with DNase digestion, and RNA concentration was evaluated using a NanoDrop Spectrophotometer (Thermo Fisher Scientific, Waltham, MA).

Whole-Transcriptome Array and RT-qPCR Validation

Selected samples were analyzed by microarray hybridization with Human Clariom D Assay kit and GeneChip WT

TABLE 1. Summary of the 30 Cases Analyzed

Case	Sex	Age	Diagnosis	PMD	RIN	TDP43
1	M	66	Control	18 h 0 min	6.4	–
2	M	61	Control	3 h 40 min	7.0	–
3	M	62	Control	5 h 45 min	5.0	–
4	M	74	Control	6 h 40 min	7.2	–
5	M	65	Control	5 h 15 min	6.8	–
6	F	64	Control	2 h 15 min	5.0	–
7	M	63	Control	8 h 05 min	7.1	–
8	F	79	Control	3 h 35 min	6.8	–
9	F	67	Control	5 h 20 min	6.2	–
10	M	70	Control	3 h 45 min	7.2	–
11	M	52	Control	4 h 40 min	7.2	–
12	F	52	Control	5 h 45 min	5.1	–
13	F	82	Control	7 h 35 min	5.2	–
14	F	74	Control	2 h 45 min	5.7	–
15	M	76	sFTLD-TDP	5 h 0 min	6.2	A
16	F	82	sFTLD-TDP	3 h 40 min	6.4	A
17	M	71	sFTLD-TDP	4 h 0 min	6.1	A
18	F	77	sFTLD-TDP	16 h 0 min	6.9	C
19	M	73	sFTLD-TDP	5 h 0 min	6.7	C
20	M	63	sFTLD-TDP	9 h 30 min	5.0	A
21	F	77	sFTLD-TDP	7 h 39 min	7.0	A
22	M	65	sFTLD-TDP	13 h 0 min	7.4	A
23	F	88	sFTLD-TDP	6 h 30 min	5.4	A
24	M	59	sFTLD-TDP	8 h 0 min	7.4	A
25	M	58	sFTLD-TDP	4 h 0 min	7.3	A
26	M	56	sFTLD-TDP	8 h 0 min	5.0	A
27	F	84	sFTLD-TDP	6 h 0 min	5.9	B
28	M	78	sFTLD-TDP	7 h 15 min	6.7	C
29	M	66	sFTLD-TDP	5 h 15 min	7.2	A
30	M	74	sFTLD-TDP	15 h 0 min	6.4	C

sFTLD-TDP, sporadic frontotemporal lobar degeneration-TDP; F, female; M, male; PM, postmortem delay; RIN, RNA integrity number; TDP43, histological types of FTLD-TDP based on TDP-43-immunoreactive inclusions (see Materials and Methods).

Plus Reagent Kit and microarray 7000 G platform from Affymetrix (Santa Clara, CA). Preprocessing of raw data and statistical analyses were performed using bioconductor packages in R programming environment for genes (22). Complementary DNA (cDNA) was obtained using High-Capacity cDNA Reverse Transcription kit (Applied Biosystems, Foster City, CA) following the protocol of the supplier. Parallel reactions for each RNA sample were run in the absence of MultiScribe Reverse Transcriptase to assess lack of contamination of genomic DNA. Gene selection was based upon their values using a test for differential expression between 2 classes (Student *t*-test). Selected genes differentially expressed showed an absolute logarithm of fold change >0.5 combined with a *p* value ≤ 0.01. Table 2 shows identification numbers and names of selected TaqMan probes. Most of the tested probes corresponded to deregulated genes as revealed by microarrays; the remainder was selected to assess other key genes of the altered pathways that were not identified as deregulated in the arrays. TaqMan RT-qPCR assays were performed in duplicate for each gene on cDNA samples in 384-well optical plates using

TABLE 2. Gene Symbols and TaqMan Probes Used in Frontal Cortex Area 8 Including Normalization Probes (*GUS-β*)

Gene	TaqMan assay
<i>ABLIM2</i>	Hs004022222_m1
<i>ACTLB6</i>	Hs00211827_m1
<i>ACTR3B</i>	Hs01051213_m1
<i>ACTR3C</i>	Hs03988416_m1
<i>AK1</i>	Hs00176119_m1
<i>AK2</i>	Hs01123132_g1
<i>AK5</i>	Hs00952786_m1
<i>AK7</i>	Hs00330574_m1
<i>AMIGO1</i>	Hs00324802_s1
<i>APOOL</i>	Hs00922772_g1
<i>APRT</i>	Hs00975725_m1
<i>ARPC5L</i>	Hs00229649_m1
<i>ATP2B3</i>	Hs00222625_m1
<i>ATP2B4</i>	Hs00608066_m1
<i>ATP4A</i>	Hs00167575_m1
<i>ATP5A1</i>	Hs00900735_m1
<i>ATP5B</i>	Hs00969569_m1
<i>ATP5H</i>	Hs01046892_gH
<i>ATP5L</i>	Hs00538946_g1
<i>ATP5O</i>	Hs00426889_m1
<i>ATP6D</i>	Hs00371515_m1
<i>ATP6V1A</i>	Hs01097169_m1
<i>BSN</i>	Hs01109152_m1
<i>C9ORF72</i>	Hs00376619_m1
<i>CALB1</i>	Hs01077197_m1
<i>CEP126</i>	Hs01573778_m1
<i>CEP41</i>	Hs00363344_m1
<i>CKAP2</i>	Hs00217068_m1
<i>COA6</i>	Hs01372973_m1
<i>CORO2A</i>	Hs00185610_m1
<i>COX7AL</i>	Hs00190880_m1
<i>DDN</i>	Hs00391784_m1
<i>DGUOK</i>	Hs00176514_m1
<i>ENTPD1</i>	Hs00969559_m1
<i>ENTPD2</i>	Hs00154301_m1
<i>ENTPD3</i>	Hs00928977_m1
<i>FASTKD2</i>	Hs01556124_m1
<i>FRMPD4</i>	Hs01568794_m1
<i>GABBR2</i>	Hs01554996_m1
<i>GABRA1</i>	Hs00971228_m1
<i>GABRA2</i>	Hs00168069_m1
<i>GABRA3</i>	Hs00968130_m1
<i>GABRB2</i>	Hs00241451_m1
<i>GABRB3</i>	Hs00241459_m1
<i>GABRD</i>	Hs00181309_m1
<i>GABRG2</i>	Hs00168093_m1
<i>GABRG3</i>	Hs00264276_m1
<i>GAD1</i>	Hs01065893_m1
<i>GAP43</i>	Hs00967138_m1
<i>GDAP1L1</i>	Hs00225209_m1
<i>GFAP</i>	Hs00909240_m1
<i>GRIAI</i>	Hs00181348_m1
<i>GRIN2A</i>	Hs00168219_m1

(continued)

TABLE 2. Continued

Gene	TaqMan assay
<i>GRIN2B</i>	Hs01002012_m1
<i>GRM5</i>	Hs00168275_m1
<i>GULP1</i>	Hs01061497_m1
<i>GUS-β</i>	Hs00939627_m1
<i>HOMER1</i>	Hs01029333_m1
<i>KIF17</i>	Hs00325418_m1
<i>KLC2</i>	Hs03988192_m1
<i>LRRC6</i>	Hs00917168_m1
<i>MAP1A</i>	Hs00357973_m1
<i>MAST3</i>	Hs00390797_m1
<i>MCU</i>	Hs00293548_m1
<i>MICU3</i>	Hs01028469_m1
<i>MRPL1</i>	Hs00220322_m1
<i>MRPS35</i>	Hs00950427_m1
<i>MTIF2</i>	Hs01091373_m1
<i>MTX3</i>	Hs01372688_m1
<i>NDUFA10</i>	Hs01071117_m1
<i>NDUFA2</i>	Hs00159575_m1
<i>NDUFA5</i>	Hs00916783_m1
<i>NDUFAF2</i>	Hs02380072_u1
<i>NDUFAF6</i>	Hs00901870_m1
<i>NDUFB10</i>	Hs00605903_m1
<i>NDUFB5</i>	Hs00159582_m1
<i>NDUFB8</i>	Hs00428204_m1
<i>NDUFS8</i>	Hs00159597_m1
<i>NME1</i>	Hs02621161_s1
<i>NME3</i>	Hs01573874_g1
<i>NME4</i>	Hs00359037_m1
<i>NME7</i>	Hs00273690_m1
<i>NRN1</i>	Hs00213192_m1
<i>NTSC</i>	Hs00274359_m1
<i>NUDT1</i>	Hs00159343_m1
<i>PAK5</i>	Hs00379318_m1
<i>PCLO</i>	Hs00382694_m1
<i>PLP1</i>	Hs00166914_m1
<i>PNP</i>	Hs01002926_m1
<i>POLR3B</i>	Hs00932002_m1
<i>PRUNE</i>	Hs00535700_m1
<i>PSD</i>	Hs00160539_m1
<i>RMND1</i>	Hs01012514_m1
<i>RMND2</i>	Hs04187037_m1
<i>RND1</i>	Hs00205507_m1
<i>SDHB</i>	Hs00268117_m1
<i>SLC17A7</i>	Hs00220404_m1
<i>SLC1A1</i>	Hs00188172_m1
<i>SLC1A2</i>	Hs01102423_m1
<i>SLC25A1</i>	Hs01105608_g1
<i>SLC25A11</i>	Hs00185940_m1
<i>SLC25A23</i>	Hs01012756_m1
<i>SLC32A1</i>	Hs00369773_m1
<i>SNAP25</i>	Hs00938957_m1
<i>SNAP91</i>	Hs01097941_m1
<i>SYN1</i>	Hs00199577_m1
<i>SYP</i>	Hs00300531_m1

(continued)

TABLE 2. Continued

Gene	TaqMan assay
<i>SYT1</i>	Hs00194572_m1
<i>TARDBP</i>	Hs00606522_m1
<i>TOMM70</i>	Hs00207896_m1
<i>UQCR11</i>	Hs00907747_m1
<i>UQCRB</i>	Hs00559884_m1
<i>VAMP1</i>	Hs04399177_m1

an ABI Prism 7900 Sequence Detection system (Applied Biosystems, Life Technologies, Waltham, MA). For each 10 μ L TaqMan reaction, 4.5 μ L cDNA was mixed with 0.5 μ L 20 \times TaqMan Gene Expression Assays and 5 μ L of 2 \times TaqMan Universal PCR Master Mix (Applied Biosystems). Values of *GUS-β* were used as internal controls for normalization (23). The parameters of the reactions were 50°C for 2 minutes, 95°C for 10 minutes, and 40 cycles of 95°C for 15 seconds and 60°C for 1 minute. Finally, capture of all TaqMan PCR data used the Sequence Detection Software (SDS version 2.2.2, Applied Biosystems). For the data analysis, threshold cycle (CT) values for each sample were processed to obtain the double delta CT ($\Delta\Delta$ CT) values. First, delta CT (Δ CT) values were calculated as the normalized CT values of each target gene in relation to the CT of endogenous controls *GUS-β*. Then, $\Delta\Delta$ CT values were obtained from the Δ CT of each sample minus the mean Δ CT of the population of control samples. Results were analyzed using the Student *t*-test.

RNA Purification, Retrotranscription Reaction, and RT-qPCR for Detection of 3 R and 4 R Tau Isoforms

Tau mRNA isoforms were assessed by using SYBR green quantitative RT-qPCR; 1000 ng of total RNA was used as a template. cDNA samples obtained from the retrotranscription reaction were diluted 1:20 and duplicate SYBR green PCR assays for each gene were performed. For each reaction, 2.5 μ L of cDNA was mixed with 1.25 μ L of forward primer 10 μ M, 1.25 μ L reverse primer 10 μ M, and 5 μ L of PowerUp SYBR Green Master Mix (Applied Biosystems). The reactions were performed following the parameters: 50°C for 2 minutes, 95°C for 10 minutes, and 40 cycles at 95°C for 15 seconds and at 60°C for 1 minute. SYBR green PCR data were captured using the Sequence Detection Software (SDS version 2.2). 3Rtau forward primer sequence: GTCCGTACTCCACC-CAAGTC; 3Rtau reverse: GTTTGTAGACTATTTG-CACCTTC; 4Rtau forward: GGCGGGAAGATGCAGATAA TTAAT; 4Rtau reverse: GTAGACTATTTGCACACTGCC. Parallel assays for each sample were carried out using primers for β -glucuronidase (*GUS-β*), forward: GTCTGCGGCA TTTTGTCCGG; reverse: CACACGATGGCATAGGAATGG as endogenous controls. Mean fold-change values of each experimental group were analyzed by 1-way ANOVA test with post hoc Tukey by using GraphPad Prism version 5.01 (La Jolla, CA) and Statgraphics Statistical Analysis and Data Visualization Software version.1 (Warrenton, VA).

TABLE 3. List of Antibodies Used in Western Blotting

Primary antibody	Symbol	Source	Reference	Host	WB Dilution
Actin Binding LIM Protein Family Member 2	ABLIM2	Abcam	ab100926	Rabbit	1:750
ATP synthase subunit alpha, mitochondrial	ATP5	Abcam	ab110411	Mouse	1:1000
Calbindin	CALB	Swant	CB-38a	Rabbit	1:5000
Chromosome 9 open reading frame 72	C9ORF72	Abcam	ab183892	Rabbit	1:500
Cytochrome b-c1 complex subunit 2, mitochondrial	UQCRC2	Abcam	ab110411	Mouse	1:1000
Cytochrome c oxidase	MT-CO1	Abcam	ab110411	Mouse	1:1000
Gamma-aminobutyric acid Receptor Subunit beta-2	GABAARB2	Abcam	ab156000	Rabbit	1:500
Gamma-Aminobutyric Acid Type A Receptor Delta Subunit	GABRD	Abcam	ab110014	Rabbit	1:1000
Glial Fibrillary Acidic Protein	GFAP	Dako	Z0334	Rabbit	1:5000
Glutamate (NMDA) receptor subunit epsilon-1	NMDAR2A	Abcam	ab169555	Rabbit	1:250
Glutamate Decarboxylase 1	GAD1	CellSignaling	#5305	Rabbit	1:250
Glyceraldehyde-3-Phosphate Dehydrogenase	GAPDH	Abcam	ab9485	Rabbit	1:2500
Mitochondrial import receptor subunit TOM70	TOMM70	Novus biological	NBP1-87863	Rabbit	1:500
NADH dehydrogenase (ubiquinone) 1 alpha subcomplex subunit 10	NDUFA10	Antibody BCN	GTX114572	Rabbit	1:1000
NADH dehydrogenase (ubiquinone) 1 beta subcomplex subunit 10	NDUFB10	Antibody BCN	15589-1-AP	Rabbit	1:2500
NADH dehydrogenase (ubiquinone) 1 beta subcomplex subunit 8, mitochondrial	NDUFB8	Abcam	ab110411	Mouse	1:1000
NADH dehydrogenase (ubiquinone) iron-sulfur protein 8, mitochondrial	NDUFS8	Antibody BCN	GTX114119	Rabbit	1:1000
NADH-ubiquinone oxidoreductase chain 1	MT-ND1	Abcam	ab181848	Rabbit	1:1000
Postsynaptic density protein 95	PSD-95	Invitrogen	7E3-1B8	Mouse	1:1000
Succinate dehydrogenase (ubiquinone) iron-sulfur subunit, mitochondrial	SDHB	Abcam	ab110411	Mouse	1:1000
Synaptophysin	SYN	Novocastra	NCL-L-SYNAP-299	Mouse	1:1000
Synaptosome Associated Protein 25	SNAP-25	BioLegend	SMI81	Mouse	1:1000
Vesicular inhibitory amino acid transporter	VGAT	Synaptic systems	131 011	Mouse	1:1000
Voltage Dependent Anion Channel 1	VDAC1	Abcam	ab15895	Rabbit	1:500
4R TAU	4R TAU	Merck-Millipore	clone 1E1/A6	Mouse	1:50
3R TAU	3R TAU	Merck-Millipore	clone 8E6/C11	Mouse	1:500
Phospho-tau Thr181	Thr181	Cell Signalling	mAb 12885	Rabbit	1:50
Total Tau	Tau 5	Thermo-Fisher	AHBOO42	Mouse	1:250
TAR DNA-binding protein 43	TDP-43	Abcam	ab154047	Rabbit	1:250

Gel Electrophoresis and Western Blotting

Frozen samples of the frontal cortex area 8 were homogenized in RIPA lysis buffer (50 mM Tris/HCl buffer, pH 7.4 containing 2 mM EDTA, 0.2% Nonidet P-40, 1 mM PMSF, protease, and phosphatase inhibitor cocktails; Roche Molecular Systems, Pleasanton, CA). Homogenates were centrifuged at 14 000g for 20 minutes. Protein concentration was determined with the BCA method (ThermoFisher Scientific). Equal amounts of protein (12 µg) for each sample were loaded and separated by electrophoresis on 10% sodium dodecyl-sulfate polyacrylamide gel electrophoresis (SDS-PAGE) gels and transferred onto nitrocellulose membranes (Amersham, Freiburg, Germany). Nonspecific binding was blocked by incubation with 3% albumin in PBS containing 0.2% Tween for 1 hour at room temperature. After washing, membranes were incubated overnight at 4°C with 1 of primary antibodies (Table 3). Protein loading was normalized using an antibody against GAPDH (37 kDa, 1:2500, Abcam, Cambridge, UK). Membranes were then incubated for 1 hour in the appropriate HRP-conjugated secondary antibodies (1:2000, Dako, Santa Clara, CA). Immunocomplexes were revealed with chemiluminescence reagent (ECL, Amersham). Densitometric quantification was carried out with ImageLab v4.5.2 software (Bio-Rad, Hercules, CA).

Isolation of Mitochondrial-Enriched Fractions From Human Brain Tissue

Mitochondria were extracted from frozen frontal cortex (100 mg) under ice-cold conditions. Tissues were minced in ice-cold isolation buffer (IB) containing 0.25 M sucrose, 10 mmol/L Tris, and 0.5 mmol/L EDTA, pH 7.4, and then homogenized and centrifuged at 1000g for 10 minutes. Samples were homogenized with a micropestle using 10 vol buffer per mg of tissue and centrifuged at 1000g for 10 minutes at 4°C. The supernatant (S1) was conserved. The pellet was washed with 2 vol IB and centrifuged under the same conditions. The last supernatant (S2) was combined with S1, mixed, and centrifuged at 10 000g for 10 minutes at 4°C, resulting in the mitochondria-enriched pellet. The supernatant (S3) was discarded and the pellet was washed with 2 volumes IB and centrifuged at 10 000g for 10 minutes at 4°C, thereby obtaining the washed mitochondria-enriched pellet. The supernatant (S4) was discarded and the final pellet was resuspended in 1 vol IB and stored at -80°C. Protein concentration was measured using a SmartSpectTMplus spectrophotometer (Bio-Rad) and the Bradford method (Merck, Darmstadt, Germany). The mitochondrial enriched fraction was used for mitochondrial enzymatic activities and for Western blotting. Protein loading (12 µg) was normalized with anti-VDAC (1:500, Abcam).

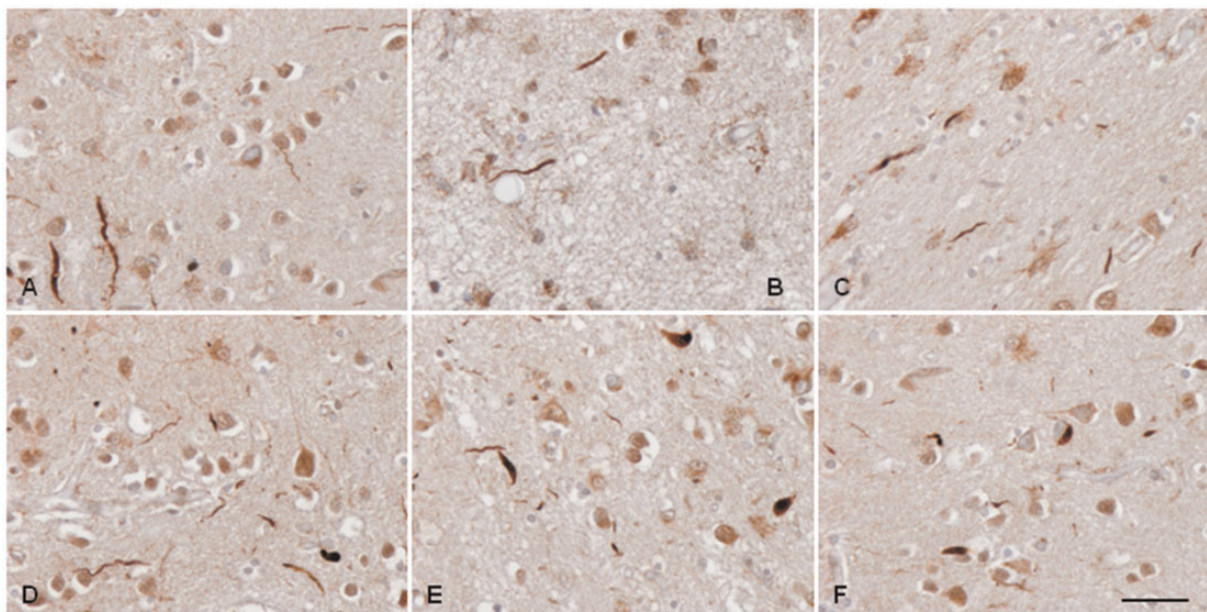


FIGURE 1. Examples of TDP-43-immunoreactive inclusions, including thin and thick dystrophic neuritis and cytoplasmic inclusions in frontal cortex area 8 in sFTLD-TDP. **(A–C)** Type C; **(D, E)** Type A; **(F)** Type B. **(A), (B), and (C)**, cases 18, 19, and 28, respectively; **(D)** and **(E)**, cases 23 and 25, respectively; **(F)**, case 27. Paraffin sections, hematoxylin counterstaining, scale bar = 50 μ m.

The activities of mitochondrial complexes I, II, IV, and V were analyzed using commercial kits following the instructions of the suppliers (Mitochondrial complex V: Novagen, Merck Biosciences; and Mitochondrial complex I, II, and IV: Abcam). Activity of citrate synthase was evaluated as a quantitative enzyme marker for the presence of intact mitochondria using commercial kits (Abcam). About 25 μ g of mitochondria extract was loaded into each well. The enzymatic activities for each mitochondrial complex were expressed as a rate of milli-optical densities per minute normalized with the citrate synthase activity.

Statistical Analysis

The normality of distribution of fold-change values was analyzed with the Kolmogorov-Smirnov test. The nonparametric Mann-Whitney test was performed to compare each group when values did not follow a normal distribution, while the unpaired *t*-test was used for normal variables. Statistical analysis and graphic design were performed with GraphPad Prism version 5.01 (La Jolla, CA). Results were analyzed with the Student *t*-test. Outliers were detected using the GraphPad software QuickCalcs ($p < 0.05$). All data were expressed as mean \pm SEM and significance levels were set at * $p < 0.05$, ** $p < 0.01$, and *** $p < 0.001$. Pearson's correlation coefficient was used to assess a possible linear association between 2 continuous quantitative variables.

RESULTS

Main Neuropathological Findings

All sFTLD-TDP cases presented variable neuron loss and microvacuolation in the upper cortical layers, mild

astrocytic gliosis in all layers of the cortex and the presence of TDP-43-immunoreactive dystrophic neurites mainly in the upper layers accompanied or not by neuronal cytoplasmic inclusions. Neuronal intranuclear inclusions were extremely rare. About 11 cases were categorized as type A, 1 as type B, and 4 as type C (Table 1; Fig. 1). Type A was characterized by numerous NCIs and DNs in the upper cortical layers; type B by numerous NCIs in the upper and inner cortical layers; and type C by predominant DNs in the upper cortical layers. p62-immunoreactive inclusions were absent in any brain region.

Microarray Analysis

All samples had enough quality for subsequent analysis after quality control analysis. The cofactors age and gender were not relevant for the analysis. After filtering, 4851 genes were included in the analysis. The analysis to select differentially expressed genes was based on adjusting a linear model with empirical Bayes moderation of the variance. The 538 top variable genes (with nominal *p* values < 0.01 and an absolute logarithm of the fold change ≥ 0.5) were represented in a heat map to illustrate common and differing gene expression patterns between control and sFTLD-TDP cases in FC (Fig. 2A). We identified 425 genes differentially expressed in sFTLD-TDP compared with controls (5 up and 420 down) (Fig. 2B). Gene Ontology (GO) database was used to highlight biological categories of differentially regulated genes. Down-regulated genes in sFTLD-TDP were involved in neurotransmission and synapsis, neuron architecture, cytoskeleton of axons and dendrites, vesicle trafficking, purine metabolism, mitochondria, and energy metabolism (Table 4). Raw data are

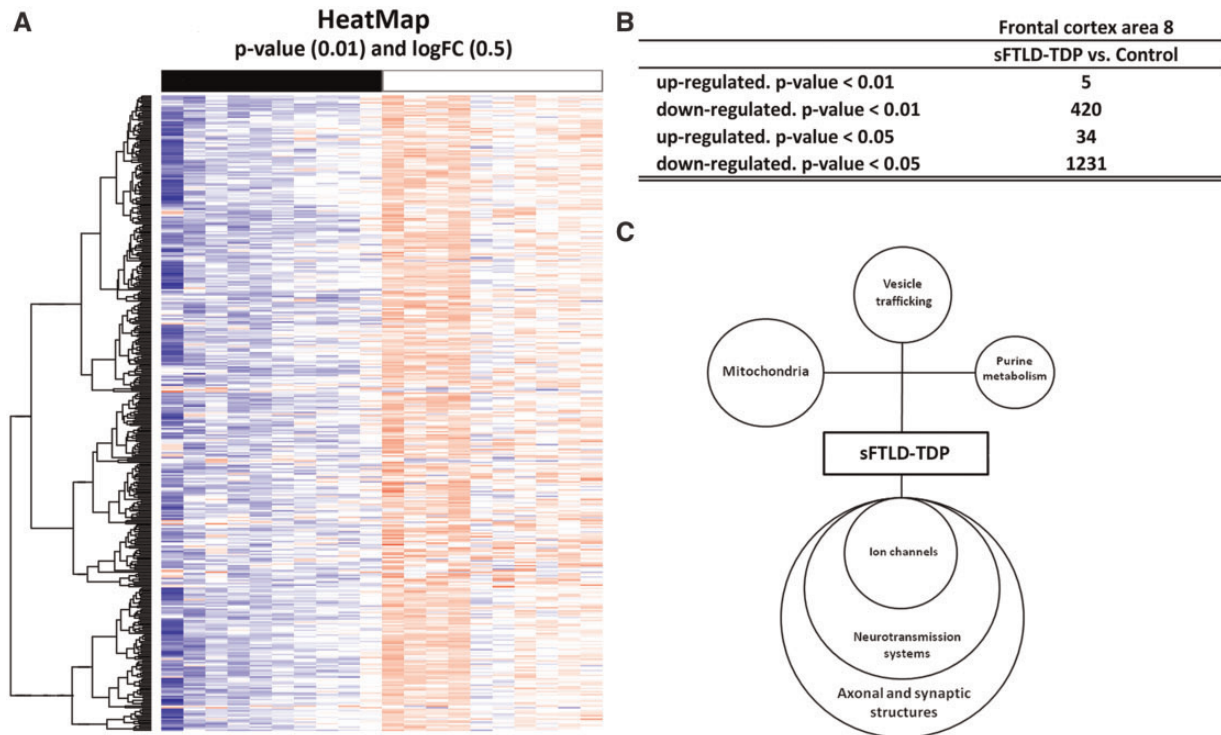


FIGURE 2. (A) Hierarchical clustering heat-map of expression intensities of mRNA array transcripts reflects differential gene expression profiles in frontal cortex area 8 in controls (red), sFTLD-TDP (blue). Differences are considered statistically significant at p value ≤ 0.01 and logFC 0.5. **(B)** Total number of significantly different expressed genes in sFTLD-TDP versus controls. **(C)** Diagram showing deregulated gene clusters in frontal cortex area 8 in sFTLD-TDP compared with controls as revealed by whole transcriptome arrays.

found in <https://www.ebi.ac.uk/arrayexpress/>; reference number fgsubs #218580.

Gene Expression Validation

RT-qPCR was carried out to assess the expression of 111 selected genes; 81 of them were abnormally regulated in sFTLD-TDP.

TARDBP and C9ORF72, and GFAP

TARDBP and C9ORF72 were significantly decreased in sFTLD-TDP compared with controls (p = 0.05 and p = 0.01, respectively) (Fig. 2A). GFAP expression was increased (p = 0.003) in sFTLD-TDP (Fig. 3A).

Cytoskeleton and Neuron Architecture

The expression of 17 genes was analyzed by RT-qPCR; 12 of them showed decreased expression in sFTLD-TDP when compared with controls. ABLIM2 (p = 0.0001), ACTLB6 (p = 0.025), ACTR3B (p = 0.002), ACTR3C (p = 0.05), CEP41 (p = 0.003), CKAP2 (p = 0.017), CORO2A (p = 0.05), KIF17 (p = 0.003), MAP1A (p = 0.05), MAST3 (p = 0.003), PAK5 (p = 0.005), and RND1 (p = 0.008) showed a significant decrease in sFTLD-TDP (Fig. 3B, C).

Synapsis and Neurotransmission

The expression of 36 genes was assessed; 30 of them were downregulated in sFTLD-TDP. The expression of the following genes implicated in presynaptic and postsynaptic attachment was significantly decreased in sFTLD-TDP: DDN (p = 0.04), FRMPD4 (p = 0.01), GAP43 (p = 0.004), HOMER1 (p = 0.000), NRN1 (p = 0.004), PCLO (p = 0.005), and PSD (p = 0.013). Similarly, 15 genes involved in GABAergic and glutamatergic neurotransmission were downregulated in sFTLD-TDP: CALB1 (p = 0.000), GABBR2 (p = 0.033), GABRA1 (p = 0.004), GABRA2 (p = 0.008), GABRA3 (p = 0.000), GABRB2 (p = 0.006), GABRB3 (p = 0.002), GABRD (p = 0.024), GABRG2 (p = 0.001), GADI (p = 0.05), GRIAI (p = 0.042), GRIN2A (p = 0.048), GRIN2B (p = 0.025), GRM5 (p = 0.002), SLC1A1 (p = 0.02), SLC17A2 (p = 0.049), and SLC32A1 (p = 0.025). Finally, a set of genes involved in synaptic vesicles were significantly deregulated in sFTLD-TDP: GULP1 (p = 0.001), SNAP25 (p = 0.006), SNAP91 (p = 0.012), SYN1 (p = 0.001), SYP (p = 0.035), and SYT1 (p = 0.017) (Fig. 4).

Expression Levels of Genes Involved in Purine Metabolism

The expression of 18 genes was assessed by RT-qPCR; 9 of them were downregulated. AK5 (p = 0.000), AK7

TABLE 4. Main Significant Clusters of Altered Genes in Frontal Cortex Area 8 in sFTLD-TDP

GO Term	Count	Size	Genes	Odds ratio	p value
Actin filament-based process	38	186	<i>ABLIM2, ACTN4, ACTR3B, ACTR3C, ADD2, ARHGEF2, ARPC5L, BAG4, BAIAP2, CACNA2D1, CACNB2, CAP2, CAPZA2, CDK5, CDK5R1, CORO2A, DNAJB6, EPB41LAB, FGF12, ID1, ITGB1BP1, LIMK1, MEF2C, PACSIN1, PHACTR1, PIP5K1C, PRKCZ, PTK2B, RND1, SCN1B, SCN2B, SCN3B, SDAD1, SORBS2, STC1, SYNPO, TPM2, WASF1</i>	1.65	6.74e-03
Action potential	15	43	<i>CACNA1G, CACNA1H, CACNA1I, CACNA2D1, CACNB2, DRD1, FGF12, GNAQ, KCNA1, PTPN3, SCN1B, SCN2A, SCN2B, SCN3B, SCN8A</i>	3.42	3.74e-04
Alternative mRNA splicing, via spliceosome	5	10	<i>CELF3, CELF4, RBFOX1, RBFOX2, RBFOX3</i>	6.30	6.82e-03
Anterograde transsynaptic signaling	63	182	<i>AKAP5, AMPH, BAIAP2, BTBD9, CA7, CACNA1G, CACNB1, CACNB2, CADPS, CADPS2, CDK5, CELF4, CHRM1, CLSTN3, DGKI, DLGAP1, DOC2A, DRD1, EGR3, FGF12, GABBR2, GABRB3, GABRG2, GFAP, GLRA3, GPR176, GRIN2A, GRM2, GRM5, GSK3A, HOMER1, HTR4, KCNA1, KCNQ2, KCNQ5, LRRTM1, LRRTM2, MAPK8IP2, MEF2C, NRXN3, OPR1, PCDH8, PIP5K1C, PLK2, PNOC, PRKCG, PRKCZ, PTK2B, RASGRF1, RIMS1, RPH3A, SCN1B, SCN2B, SLC12A5, SLC17A7, SNAP25, SNAP91, STXBPI, SYNI, SYNJI, SYP, SYT1, UNC13A</i>	3.65	1.90e-13
Axon	47	127	<i>AMIGO1, AP1S1, AP3S1, AT1L1, ATP1A3, BLOC1S2, CCK, CDK5, CDK5R1, CHRM1, DAGLA, DGKI, ELK1, GABRA2, GABRG2, GAP43, GRM2, HOMER1, HPCA, INPP5F, KCNA1, KCNA3, KCNA4, KCNC2, KCNIP3, KCNQ2, LRRTM1, NEFL, NEFM, NRP1, PACSIN1, PNOC, PRKCZ, PTK2B, ROBO2, SCN1B, SCN2A, SCN8A, SERPINF1, SLC17A7, STXBPI, SYNI, SYNJI, SYP, SYT1, UNC13A, VAMP1</i>	3.96	1.99e-11
Axon hillock	3	4	<i>CCK, PRKCZ, SERPINF1</i>	18.80	9.40e-03
Axon part	27	71	<i>AP1S1, AP3S1, BLOC1S2, CCK, CHRM1, DAGLA, DGKI, ELK1, KCNA1, KCNC2, KCNIP3, KCNQ2, NEFL, PACSIN1, PNOC, PRKCZ, ROBO2, SCN1B, SCN2A, SCN8A, SERPINF1, STXBPI, SYNI, SYNJI, SYP, SYT1, VAMP1</i>	4.00	2.42e-07
Axon terminus	16	35	<i>AP1S1, CCK, CHRM1, DGKI, ELK1, KCNA1, KCNC2, KCNIP3, PACSIN1, PNOC, STXBPI, SYNI, SYNJI, SYP, SYT1, VAMP1</i>	5.40	4.44e-06
Blood circulation	30	138	<i>ATP1A3, ATP2B1, CACNA1G, CACNA1H, CACNA2D1, CACNB1, CACNB2, CACNG2, CACNG3, CHRM1, CLIC2, DRD1, EHD3, FGF12, GSK3A, HMGCGR, ITGB1BP1, KCND3, KCNIP1, KCNIP3, KCNIP4, KCNK1, NCALD, OPR1, PPARG, SCN1B, SCN2B, SCN3B, STC1, TRHDE</i>	1.78	6.23e-03
Calcium channel complex	10	26	<i>CACNA1G, CACNA1H, CACNA1I, CACNA2D1, CACNB1, CACNB2, CACNG2, CACNG3, MCU, PTPA</i>	3.96	1.53e-03
Calcium ion binding	38	171	<i>ACTN4, ANXA2, CABP1, CAMKK2, CDH10, CDH12, CDH18, CDH9, CDK5R1, CLSTN3, CRTAC1, DGKB, DOC2A, EHD3, EPDR1, HPCA, KCNIP1, KCNIP3, KCNIP4, MCTP1, NCALD, NELL1, PCDH19, PCDH8, PITPNM2, PITPNM3, PPP3R1, PRSS3, RASGRP1, RCVRN, REPS2, RPH3A, SLC25A23, SLIT1, SYTI, TBC1D9, TLL1, VSNL1</i>	1.85	1.44e-03
Calcium ion transmembrane transporter activity	11	37	<i>ATP2B1, CACNA1G, CACNA1H, CACNA1I, CACNA2D1, CACNB1, CACNB2, CACNG2, CACNG3, GRIN2A, MCU</i>	2.68	8.89e-03
Channel activity	42	139	<i>CACNA1G, CACNA1H, CACNA1I, CACNA2D1, CACNB1, CACNB2, CACNG2, CACNG3, CLIC2, GABRA2, GABRA3, GABRB3, GABRG2, GABRG3, GLRA3, GRIN2A, KCNA1, KCNA3, KCNA4, KCNB2, KCNC2, KCND3, KCNIP1, KCNIP3, KCNIP4, KCNJ16, KCNJ6, KCNK1, KCNQ2, KCNQ5, KCNS2, KCNV1, MCU, NCALD, PTK2B, SCN1B, SCN2A, SCN2B, SCN3B, SCN8A, SLC17A7, TTYH3</i>	2.87	2.44e-07
Chemical synaptic transmission, postsynaptic	12	22	<i>CDK5, CELF4, DGKI, GABRB3, GRIN2A, GSK3A, MAPK8IP2, MEF2C, PRKCZ, PTK2B, RIMS1, SLC17A7</i>	7.65	7.33e-06

(continued)

TABLE 4. Continued

GO Term	Count	Size	Genes	Odds ratio	p value
Chloride channel complex	8	19	<i>CLIC2, GABRA2, GABRA3, GABRB3, GABRG2, GABRG3, GLRA3, TTYH3</i>	4.60	2.33e-03
Cilium	23	88	<i>ANKMY2, ARL6, C5orf30, CEP126, CEP41, CFAP221, DRD1, EHD3, GNAQ, GPR83, GRK4, HK1, IQUB, KIF17, KIFAP3, LRRC6, MCHR1, NAPEPLD, NME5, PRKAR1B, PRKAR2B, SSX2IP, WRAP73</i>	2.27	1.39e-04
Circulatory system process	30	138	<i>ATP1A3, ATP2B1, CACNA1G, CACNA1H, CACNA2D1, CACNB1, CACNB2, CACNG2, CACNG3, CHRM1, CLIC2, DRD1, EHD3, FGF12, GSK3A, HMGR, ITGB1BP1, KCND3, KCNIP1, KCNIP3, KCNIP4, KCNK1, NCALD, OPR1, PPARG, SCN1B, SCN2B, SCN3B, STC1, TRHDE</i>	1.78	6.23e-03
Cyclic nucleotide biosynthetic process	13	38	<i>CAP2, ADCY1, RUNDC3A, DRD1, PTK2B, GNAL, GRM2, GSK3A, HPCA, OPR1</i>	3.31	1.13e-03
Cyclic purine nucleotide metabolic process	13	38	<i>CAP2, ADCY1, RUNDC3A, DRD1, PTK2B, GNAL, GRM2, GSK3A, HPCA, OPR1</i>	3.31	1.13e-03
Dendrite	43	160	<i>AMIGO1, ARHGAP32, ARHGAP44, ARHGEF2, ATP1A3, BAIAP2, CCK, CDK5, CDK5R1, CHLI, CHRM1, DGKI, DRP2, ELK1, FRMPD4, GABRA2, GLRA3, GLRX2, GNAQ, GNG3, GRK4, GRM2, HPCA, INPP5F, KCNA1, KCNB2, KCNC2, KCND3, KCNIP1, KCNIP3, KCNK1, PCDH8, PCSK2, PLK2, PNO, PRKAR2B, PRKCG, PTK2B, RCVRN, SLC12A5, SYN1, SYNPO, THY1</i>	2.42	5.82e-06
Dendrite extension	4	7	<i>CPNE5, RIMS1, SYT1, UNC13A</i>	8.38	8.91e-03
Dopamine receptor signaling pathway	5	9	<i>DRD1, GNAL, GNAQ, GSK3A, VPS35</i>	7.87	3.84e-03
GABA receptor activity	6	10	<i>GABBR2, GABRA2, GABRA3, GABRB3, GABRG2, GABRG3</i>	9.47	8.64e-04
GABA receptor complex	5	9	<i>GABRA2, GABRA3, GABRB3, GABRG2, GABRG3</i>	7.87	3.84e-03
Gamma-aminobutyric acid signaling pathway	6	10	<i>HTR4, GABRG3, GABRG2, GABRA3, GABRA2, GABBR2</i>	9.47	8.64e-04
Glutamate receptor signaling pathway	13	28	<i>ATP1A3, CACNG2, CACNG3, CDK5R1, GNAQ, GRIN2A, GRM2, GRM5, HOMER1, MAPK8IP2, MEF2C, PTK2B, RASGRF1</i>	5.53	2.93e-05
Glutamate secretion	7	15	<i>CCK, GRM2, RIMS1, SLC17A7, SNAP25, STXB1, SYT1</i>	5.53	2.14e-03
Growth cone	13	41	<i>CDK5, CDK5R1, CRTAC1, GAP43, LRRTM1, NEFL, NGEF, NRP1, PTK2B, RASGRF1, SNAP25, THY1, TIAM2</i>	2.95	2.48e-03
Intracellular protein transport	46	237	<i>AKAP5, ANXA2, AP1S1, AP2S1, AP3S1, ARHGEF2, ARL6, ATG4B, BAG4, BAP1, BID, CABP1, CDK5, CDK5R1, CHML, CHRM1, DRD1, EHD3, FBXW7, GDAP1, GNAQ, GSK3A, HPCA, ITGB1BP1, KCNB2, KCNIP3, MAPK14, NAPB, NAPG, OAZ2, PPP3R1, RAB8B, RANBP1, REEP2, RFTN1, RIMS1, RPH3A, RTN2, SSX2IP, TBC1D9, TMEM30A, TOMM34, TOMM70, UBR5, VPS35, VPS36</i>	1.56	8.18e-03
Ion channel complex	46	96	<i>AMIGO1, CACNA1G, CACNA1H, CACNA1I, CACNA2D1, CACNB1, CACNB2, CACNG2, CACNG3, CLIC2, DPP6, GABRA2, GABRA3, GABRB3, GABRG2, GABRG3, GLRA3, GRIN2A, KCNA1, KCNA3, KCNA4, KCNB2, KCNC2, KCND3, KCNIP1, KCNIP3, KCNIP4, KCNJ16, KCNJ6, KCNK1, KCNQ2, KCNQ5, KCNS2, KCNV1, MCU, OLFM2, OLFM3, PTK2B, PTPA, SCN1B, SCN2A, SCN2B, SCN3B, SCN8A, SNAP25, TTYH3</i>	6.24	3.15e-16
Ionotropic glutamate receptor signaling pathway	4	7	<i>ATP1A3, CDK5R1, GRIN2A, PTK2B</i>	8.38	8.91e-03
Main axon	9	25	<i>CCK, DAGLA, KCNA1, KCNC2, KCNQ2, ROBO2, SCN1B, SCN2A, SCN8A</i>	3.56	4.44e-03
Mitochondrial outer membrane permeabilization	4	7	<i>BID, BLOC1S2, GSK3A, PPP3R1</i>	8.38	8.91e-03
Mitochondrial outer membrane permeabilization involved in programmed cell death	4	7	<i>BID, BLOC1S2, GSK3A, PPP3R1</i>	8.38	8.91e-03

(continued)

TABLE 4. Continued

GO Term	Count	Size	Genes	Odds ratio	p value
Modulation of synaptic transmission	27	78	<i>BAIAP2, BTBD9, CA7, CDK5, CELF4, CLSTN3, DGKI, DRD1, GFAP, GRIN2A, GRM2, GRM5, LRRTM1, LRRTM2, MAPK8IP2, MEF2C, PLK2, PRKCZ, PTK2B, RASGRF1, RIMS1, SNAP25, STXBP1, SYN1, SYP, SYT1, UNC13A</i>	3.44	2.13e-06
Neurofilament	4	6	<i>INA, NEFL, NEFM, NRP1</i>	12.60	4.28e-03
Neuron part	107	379	<i>ACTL6B, ACTN4, ADGRB1, AMIGO1, AMPH, AP1S1, AP3S1, ARHGAP32, ARHGAP44, ARHGEF2, ATLI, ATP1A3, ATP2B1, BAIAP2, BLOC1S2, CABP1, CADPS, CADPS2, CCK, CDK5, CDK5R1, CHL1, CHRM1, CPNE5, CRTAC1, DAGLA, DDN, DGKI, DLGAP1, DOC2A, DRP2, ELK1, ENC1, FRMPD4, GABBR2, GABRA2, GABRG2, GAP43, GLRA3, GLRX2, GNAQ, GNG3, GRIN2A, GRK4, GRM2, GRM5, HOMER1, HPCA, ICA1, INPP5F, KCNA1, KCNA3, KCNA4, KCNB2, KCNC2, KCND3, KCNIP1, KCNIP3, KCNK1, KCNQ2, LIMK1, LRRTM1, MAPK8IP2, NAPEPLD, NEFL, NEFM, NGEF, NRP1, NRSN2, NRXN3, OPRL1, PACSIN1, PCDH8, PCSK2, PDE1B, PIP5K1C, PLK2, PNOC, PRKAR2B, PRKCG, PRKCZ, PTK2B, RAP1GAP2, RASGRF1, RBFOX3, RCVRN, RIMS1, ROBO2, RPH3A, SCN1B, SCN2A, SCN8A, SERPINF1, SLC12A5, SLC17A7, SNAP25, STXBP1, SV2B, SYN1, SYNJ1, SYNPO, SYP, SYT1, THY1, TIAM2, UNC13A, VAMP1</i>	2.81	2.92e-15
Neuron projection	90	294	<i>ACTN4, AMIGO1, AP1S1, AP3S1, ARHGAP32, ARHGAP44, ARHGEF2, ATLI, ATP1A3, ATP2B1, BAIAP2, BLOC1S2, CCK, CDK5, CDK5R1, CHL1, CHRM1, CPNE5, CRTAC1, DAGLA, DDN, DGKI, DOC2A, DRP2, ELK1, FRMPD4, GABBR2, GABRA2, GABRG2, GAP43, GLRA3, GLRX2, GNAQ, GNG3, GRIN2A, GRK4, GRM2, GRM5, HOMER1, HPCA, INPP5F, KCNA1, KCNA3, KCNA4, KCNB2, KCNC2, KCND3, KCNIP1, KCNIP3, KCNK1, KCNQ2, LIMK1, LRRTM1, NEFL, NEFM, NGEF, NRP1, OPRL1, PACSIN1, PCDH8, PCSK2, PLK2, PNOC, PRKAR2B, PRKCG, PRKCZ, PTK2B, RAP1GAP2, RASGRF1, RCVRN, ROBO2, RPH3A, SCN1B, SCN2A, SCN8A, SERPINF1, SLC12A5, SLC17A7, SNAP25, STXBP1, SV2B, SYN1, SYNJ1, SYNPO, SYP, SYT1, THY1, TIAM2, UNC13A, VAMP1</i>	3.16	3.62e-15
Neuron projection morphogenesis	33	157	<i>ADCY1, ADGRB1, AMIGO1, ATLI, BAIAP2, CCK, CDK5, CDK5R1, CHL1, CHN1, CPNE5, GAP43, HPRT1, ID1, LIMK1, MAPK8IP2, NEFL, NGEF, NRP1, NRXN3, NTN4, PACSIN1, PRKCZ, RBFOX2, RIMS1, ROBO2, SCN1B, SLIT1, STXBP1, SYT1, THY1, UNC13A, ZNF280B</i>	1.71	7.27e-03
Neuron remodeling	3	4	<i>GNAQ, NTN4, RND1</i>	18.80	9.40e-03
Neuronal cell body	36	130	<i>AMIGO1, ARHGEF2, ATP2B1, BAIAP2, CCK, CDK5, CDK5R1, CPNE5, DDN, DGKI, DRP2, ELK1, ENC1, GABRA2, GLRA3, GLRX2, GRK4, HPCA, INPP5F, KCNA1, KCNB2, KCNC2, KCNK1, MAPK8IP2, NRP1, NRSN2, PCSK2, PDE1B, PNOC, PRKAR2B, PRKCZ, PTK2B, RBFOX3, SERPINF1, SLC12A5, SYNPO</i>	2.50	1.69e-05
Neuron-neuron synaptic transmission	16	46	<i>CA7, CDK5, CLSTN3, DGKI, DRD1, GABRG2, GLRA3, GRM2, GRM5, MAPK8IP2, MEF2C, PTK2B, SLC17A7, STXBP1, SYT1, UNC13A</i>	4.10	5.04e-05
Neurotransmitter receptor activity	9	23	<i>CHRM1, DRD1, GABRA2, GABRA3, GABRB3, GABRG2, GLRA3, GRIN2A, PTK2B</i>	4.07	2.23e-03
Neurotransmitter secretion	16	46	<i>CDK5, RPH3A, RIMS1, UNC13A, PIP5K1C, MEF2C, SNAP25, STXBP1, SYN1, SYT1, DOC2A, CADPS, SYNJ1, DGKI, CADPS2, NRXN3</i>	3.41	2.49e-04
Node of Ranvier	4	6	<i>KCNQ2, SCN1B, SCN2A, SCN8A</i>	12.60	4.28e-03
Nonmotile primary cilium	9	25	<i>C5orf30, DRD1, GNAQ, GPR83, GRK4, KIF17, KIFAP3, MCHR1, NAPEPLD</i>	3.56	4.44e-03
Postsynapse	39	121	<i>ADGRB1, ARHGAP32, ARHGAP44, ATP1A3, BAIAP2, CABP1, CADPS2, CDK5, CDK5R1, CHRM1, CLSTN3, DGKI, DLGAP1, DRP2, FRMPD4, GABBR2, GABRA2, GABRA3, GABRB3, GABRG2, GABRG3, GAP43, GLRA3, GRIN2A, GRM5, GSK3A, HOMER1, HPCA, KCNC2, LRRTM1, LRRTM2, MAPK8IP2, MEF2C, PCDH8, PRKAR2B, PTK2B, SLC17A7, SYN1, SYNPO</i>	3.14	9.97e-08

(continued)

TABLE 4. Continued

GO Term	Count	Size	Genes	Odds ratio	p value
Postsynaptic density	17	54	<i>ADGRB1, ARHGAP32, BAIAP2, CABP1, CDK5, CDK5R1, CHRM1, DLGAP1, DRP2, GAP43, GRIN2A, GRM5, HOMER1, MAPK8IP2, PTK2B, SYNI, SYNPO</i>	2.94	6.16e-04
Potassium channel activity	16	39	<i>KCNA1, KCNA3, KCNA4, KCNB2, KCNC2, KCND3, KCNIP1, KCNIP3, KCNIP4, KCNJ16, KCNJ6, KCNK1, KCNQ2, KCNQ5, KCNS2, KCNV1</i>	4.46	2.41e-05
Potassium ion transport	25	71	<i>AMIGO1, ATP1A3, CAB39, DPP10, DPP6, DRD1, KCNA1, KCNA3, KCNA4, KCNB2, KCNC2, KCND3, KCNIP1, KCNIP3, KCNIP4, KCNJ16, KCNJ6, KCNK1, KCNQ2, KCNQ5, KCNS2, KCNV1, PTK2B, SLC12A5, SLC12A8</i>	3.52	3.60e-06
Presynapse	29	84	<i>AMPH, AP1S1, CADPS, CADPS2, CCK, CDK5, DGKI, DOC2A, GABRA2, GRIN2A, GRM2, ICA1, KCNA1, KCNC2, NRXN3, PCDH8, PIP5K1C, RIMS1, RPH3A, SLC17A7, SNAP25, STXBPI, SV2B, SYNI, SYNJ1, SYP, SYTI, UNC13A, VAMP1</i>	3.44	9.43e-07
Primary cilium	11	37	<i>ARL6, C5orf30, CEP41, DRD1, GNAQ, GPR83, GRK4, KIF17, KIFAP3, MCHR1, NAPEPLD</i>	2.68	8.98e-03
Purine nucleotide biosynthetic process	16	59	<i>ADCY1, AKAP5, ATP5A1, CAP2, DRD1, GABBR2, GNAL, GRM2, GSK3A, HPCA, HPRT1, NME5, OPRL1, PTK2B, RCVRN, RUNDC3A</i>	2.37	4.90e-03
Regulation of alternative mRNA splicing, via spliceosome	5	10	<i>CELF3, CELF4, RBFOX1, RBFOX2, RBFOX3</i>	6.30	6.82e-03
Regulation of calcium ion-dependent exocytosis	9	24	<i>CACNA1G, CACNA1I, CDK5, DOC2A, RIMS1, RPH3A, STXBPI, SYNI, SYTI</i>	3.80	3.23e-03
Regulation of ion transmembrane transport	46	125	<i>ACTN4, AMIGO1, CAB39, CACNA1G, CACNA1H, CACNA1I, CACNA2D1, CACNB1, CACNB2, CACNG2, CACNG3, CLIC2, DPP10, DPP6, DRD1, EHD3, FGF12, HOMER1, KCNA1, KCNA3, KCNA4, KCNB2, KCNC2, KCND3, KCNIP1, KCNIP3, KCNIP4, KCNJ16, KCNJ6, KCNQ2, KCNQ5, KCNS2, KCNV1, MAPK8IP2, MEF2C, MMP9, OPRL1, PTK2B, PTPN3, RASGRF1, SCN1B, SCN2A, SCN2B, SCN3B, SCN8A, THY1</i>	3.91	4.16e-11
Regulation of neurotransmitter levels	23	64	<i>CADPS, CADPS2, CDK5, DAGLA, DGKI, DOC2A, DRD1, GABRA2, GFAP, MEF2C, NRXN3, PDE1B, PIP5K1C, RIMS1, RPH3A, SLC17A7, SNAP25, STXBPI, SV2B, SYNI, SYNJ1, SYTI, UNC13A</i>	3.63	5.98e-06
Regulation of nucleotide biosynthetic process	13	37	<i>ADCY1, AKAP5, CAP2, DRD1, GABBR2, GNAL, GRM2, GSK3A, HPCA, OPRL1, PTK2B, RCVRN, RUNDC3A</i>	3.45	8.49e-04
Regulation of nucleotide metabolic process	15	49	<i>ADCY1, AKAP5, CAP2, DRD1, GABBR2, GNAL, GRM2, GSK3A, HPCA, OPRL1, PTK2B, RCVRN, RUNDC3A, SLC25A23, TIGAR</i>	2.81	1.76e-03
Regulation of purine nucleotide biosynthetic process	13	39	<i>CAP2, ADCY1, RUNDC3A, DRD1, PTK2B, GNAL, GRM2, GSK3A, HPCA, OPRL1</i>	3.18	1.49e-03
Regulation of synapse assembly	10	27	<i>ADGRB1, ADGRB2, AMIGO1, CLSTN3, LRRTM1, LRRTM2, MEF2C, NRXN3, ROBO2, SLIT1</i>	3.73	2.17e-03
Regulation of synapse organization	11	36	<i>ADGRB1, ADGRB2, AMIGO1, CLSTN3, FRMPD4, LRRTM1, LRRTM2, MEF2C, NRXN3, ROBO2, SLIT1</i>	2.79	7.18e-03
Regulation of synapse structure or activity	11	36	<i>ADGRB1, ADGRB2, AMIGO1, CLSTN3, FRMPD4, LRRTM1, LRRTM2, MEF2C, NRXN3, ROBO2, SLIT1</i>	2.79	7.18e-03
Regulation of synaptic plasticity	18	43	<i>BAIAP2, CDK5, DGKI, DRD1, GFAP, GRIN2A, GRM5, LRRTM1, LRRTM2, MEF2C, PLK2, PRKCZ, PTK2B, RASGRF1, SNAP25, STXBPI, SYP, UNC13A</i>	4.63	5.26e-06
Regulation of transmembrane transport	47	129	<i>ACTN4, AMIGO1, CAB39, CACNA1G, CACNA1H, CACNA1I, CACNA2D1, CACNB1, CACNB2, CACNG2, CACNG3, CLIC2, DPP10, DPP6, DRD1, EHD3, FGF12, HOMER1, KCNA1, KCNA3, KCNA4, KCNB2, KCNC2, KCND3, KCNIP1, KCNIP3, KCNIP4, KCNJ16, KCNJ6, KCNQ2, KCNQ5, KCNS2, KCNV1, MAPK8IP2, MEF2C, MMP9, OAZ2, OPRL1, PTK2B, PTPN3, RASGRF1, SCN1B, SCN2A, SCN2B, SCN3B, SCN8A, THY1</i>	3.86	3.79e-11

(continued)

TABLE 4. Continued

GO Term	Count	Size	Genes	Odds ratio	p value
Regulation of vesicle-mediated transport	27	120	<i>ACTN4, ANXA2, AP2S1, BTBD9, CACNA1G, CACNA1I, CADPS2, CDK5, DOC2A, INPP5F, LRRTM1, LRRTM2, NRP1, PACSIN1, PPARG, PRKCG, RAB27B, RIMS1, RINT1, RPH3A, SCFD1, SNAP91, STXBPI, SYNI, SYTI, TBC1D9, VSNL1</i>	1.86	5.74e-03
Somatodendritic compartment	54	205	<i>AMIGO1, ARHGAP32, ARHGAP44, ARHGEF2, ATP1A3, ATP2B1, BAIAP2, CCK, CDK5, CDK5R1, CHL1, CHRM1, CPNE5, DDN, DGKI, DRP2, ELK1, ENCI, FRMPD4, GABRA2, GLRA3, GLRX2, GNAQ, GNG3, GRK4, GRM2, HPCA, INPP5F, KCNA1, KCNB2, KCNC2, KCND3, KCNIP1, KCNIP3, KCNK1, MAPK8IP2, NRP1, NRSN2, PCDH8, PCSK2, PDE1B, PLK2, PNOC, PRKAR2B, PRKCG, PRKCZ, PTK2B, RBFOX3, RCVRN, SERPINF1, SLC12A5, SYNI, SYNPO, THY1</i>	2.39	6.48e-07
Synapse	68	222	<i>ADGRB1, AMPH, AP1S1, ARHGAP32, ARHGAP44, ATP1A3, ATP2B1, BAIAP2, CABP1, CADPS, CADPS2, CCK, CDK5, CDK5R1, CHRM1, CLSTN3, DDN, DGKI, DLGAP1, DOC2A, DRP2, FRMPD4, GABBR2, GABRA2, GABRA3, GABRB3, GABRG2, GABRG3, GAP43, GLRA3, GRIN2A, GRM2, GRM5, GSK3A, HOMER1, HPCA, ICA1, KCNA1, KCNC2, KCNK1, LRRTM1, LRRTM2, MAPK8IP2, MEF2C, NRXN3, OLFM2, OLFM3, PACSIN1, PCDH8, PHACTR1, PIP5K1C, PRKAR2B, PRKCG, PTK2B, RIMS1, RPH3A, SLC17A7, SNAP25, STXBPI, SV2B, SYNI, SYNJ1, SYNPO, SYP, SYTI, UNC13A, VAMP1, WASF1</i>	3.05	1.43e-11
Synapse assembly	12	39	<i>ADGRB1, ADGRB2, AMIGO1, CDK5, CLSTN3, DRD1, LRRTM1, LRRTM2, MEF2C, NRXN3, ROBO2, SLIT1</i>	2.82	4.75e-03
Synapse organization	18	67	<i>ADGRB1, ADGRB2, AMIGO1, CACNB1, CACNB2, CACNG2, CDK5, CLSTN3, DRD1, DRP2, FRMPD4, LRRTM1, LRRTM2, MEF2C, NRXN3, ROBO2, SLIT1, UNC13A</i>	2.34	3.25e-03
Synapse part	63	190	<i>ADGRB1, AMPH, AP1S1, ARHGAP32, ARHGAP44, ATP1A3, ATP2B1, BAIAP2, CABP1, CADPS, CADPS2, CCK, CDK5, CDK5R1, CHRM1, CLSTN3, DDN, DGKI, DLGAP1, DOC2A, DRP2, FRMPD4, GABBR2, GABRA2, GABRA3, GABRB3, GABRG2, GABRG3, GAP43, GLRA3, GRIN2A, GRM2, GRM5, GSK3A, HOMER1, HPCA, ICA1, KCNA1, KCNC2, LRRTM1, LRRTM2, MAPK8IP2, MEF2C, NRXN3, OLFM2, PCDH8, PIP5K1C, PRKAR2B, PRKCG, PTK2B, RIMS1, RPH3A, SLC17A7, SNAP25, STXBPI, SV2B, SYNI, SYNJ1, SYNPO, SYP, SYTI, UNC13A, VAMP1</i>	3.41	1.79e-12
Synaptic membrane	35	89	<i>ARHGAP32, ATP2B1, CABP1, CADPS2, CDK5, CHRM1, CLSTN3, DDN, DGKI, DLGAP1, DRP2, GABBR2, GABRA2, GABRA3, GABRB3, GABRG2, GABRG3, GLRA3, GRIN2A, GRM2, HOMER1, KCNA1, KCNC2, LRRTM1, LRRTM2, OLFM2, PCDH8, PRKCG, RIMS1, SNAP25, SYNJ1, SYNPO, SYP, SYTI, UNC13A</i>	4.28	1.28e-08
Synaptic signaling	63	182	<i>AKAP5, AMPH, BAIAP2, BTBD9, CA7, CACNA1G, CACNB1, CACNB2, CADPS, CADPS2, CDK5, CELF4, CHRM1, CLSTN3, DGKI, DLGAP1, DOC2A, DRD1, EGR3, FGF12, GABBR2, GABRB3, GABRG2, GFAP, GLRA3, GPR176, GRIN2A, GRM2, GRM5, GSK3A, HOMER1, HTR4, KCNA1, KCNQ2, KCNQ5, LRRTM1, LRRTM2, MAPK8IP2, MEF2C, NRXN3, OPR1, PCDH8, PIP5K1C, PLK2, PNOC, PRKCG, PRKCZ, PTK2B, RASGRF1, RIMS1, RPH3A, SCN1B, SCN2B, SLC12A5, SLC17A7, SNAP25, SNAP91, STXBPI, SYNI, SYNJ1, SYP, SYTI, UNC13A</i>	3.65	1.90e-13
Synaptic transmission, glutamatergic	12	26	<i>CDK5, CLSTN3, DGKI, DRD1, GRM2, GRM5, MAPK8IP2, MEF2C, PTK2B, SLC17A7, SYTI, UNC13A</i>	5.46	6.45e-05
Synaptic vesicle	14	37	<i>AMPH, DGKI, DOC2A, GABRA2, GRIN2A, ICA1, RPH3A, SLC17A7, SNAP25, SV2B, SYNI, SYP, SYTI, VAMP1</i>	3.88	2.21e-04
Synaptic vesicle endocytosis	6	10	<i>CDK5, BTBD9, PIP5K1C, PACSIN1, SYTI, SYNJ1</i>	9.47	8.64e-04

(continued)

TABLE 4. Continued

GO Term	Count	Size	Genes	Odds ratio	p value
Synaptic vesicle exocytosis	13	34	CADPS, CADPS2, CDK5, DOC2A, PIP5K1C, RIMS1, RPH3A, SNAP25, STXBP1, SYNI, SYNJI, SYTI, UNC13A	3.94	3.28e-04
Synaptic vesicle maturation	4	5	UNC13A, SYP, STXBP1, SLC17A7	25.20	1.60e-03
Synaptic vesicle membrane	11	22	AMPH, DOC2A, GABRA2, ICA1, RPH3A, SLC17A7, SV2B, SYNI, SYP, SYTI, VAMP1	6.36	5.22e-05
Synaptic vesicle priming	5	7	CADPS, CADPS2, SNAP25, STXBP1, SYNJI	15.80	8.14e-04
Synaptic vesicle recycling	6	10	CDK5, BTBD9, PIP5K1C, PACSINI, SYTI, SYNJI	9.47	8.64e-04
Synaptic vesicle transport	17	42	AP3S1, BLOC1S2, BTBD9, CADPS, CADPS2, CDK5, DOC2A, PACSINI, PIP5K1C, RIMS1, RPH3A, SNAP25, STXBP1, SYNI, SYNJI, SYTI, UNC13A	4.36	1.66e-05
Terminal bouton	9	17	AP1S1, CCK, KCNC2, STXBP1, SYNI, SYNJI, SYP, SYTI, VAMP1	7.14	1.47e-05
Transport vesicle	25	103	AMPH, AP1S1, AP3S1, CNST, DDHD2, DGKI, DOC2A, GABRA2, GRIN2A, ICA1, NCALD, NRSN2, PCSK2, RAB27B, RPH3A, SCG3, SLC17A7, SNAP25, STEAP2, SV2B, SYNI, SYP, SYTI, TMEM30A, VAMP1	2.06	2.69e-03
Voltage-gated ion channel activity	30	65	CACNA1G, CACNA1H, CACNA1I, CACNA2D1, CACNB1, CACNB2, CACNG2, CACNG3, CLIC2, KCNA1, KCNA3, KCNA4, KCNB2, KCNC2, KCND3, KCNIP1, KCNIP3, KCNIP4, KCNJ16, KCNJ6, KCNK1, KCNQ2, KCNQ5, KCNS2, KCNV1, SCN1B, SCN2A, SCN2B, SCN3B, SCN8A	5.64	1.91e-10

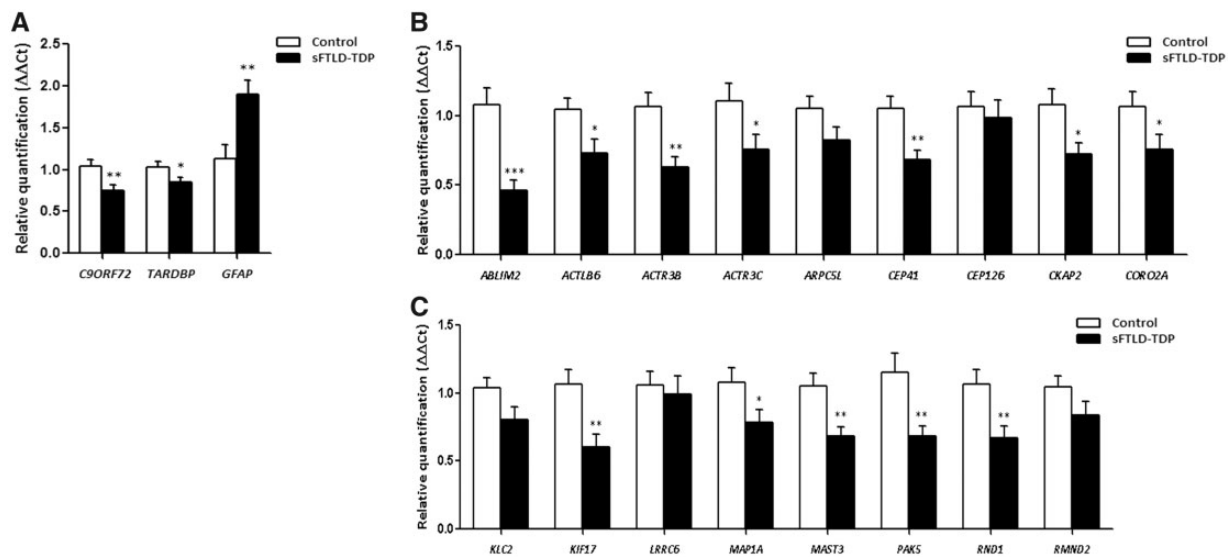


FIGURE 3. mRNA expression levels of selected deregulated genes in frontal cortex area 8 of sFTLD-TDP and controls assessed with TaqMan RT-qPCR assays. Genes coding for (A) proteins involved in toxic aggregates of FTL variants and GFAP; (B, C) cytoskeleton and structural components. Significant levels set at * $p < 0.05$, ** $p < 0.01$, and *** $p < 0.001$.

($p = 0.001$), *APRT* ($p = 0.001$), *DGUOK* ($p = 0.007$), *ENTPD3* ($p = 0.02$), *NME1* ($p = 0.03$), *NME3* ($p = 0.01$), *NME7* ($p = 0.007$), and *POLR3B* ($p = 0.003$) were significantly deregulated in sFTLD-TDP (Fig. 5).

Protein Expression Levels of Selected Genes

Expression levels of 14 proteins not related to mitochondria and energy metabolism were assessed. C9ORF72 protein

levels were significantly decreased in sFTLD-TDP ($p = 0.01$). However, TDP-43 levels were increased in sFTLD-TDP ($p = 0.02$) (Fig. 6). Significant reduction of VGAT ($p = 0.04$) and GAD1 ($p = 0.02$) levels occurred in sFTLD-TDP. A significant reduction was found in GABRD protein levels ($p = 0.02$), but no changes were detected in synaptophysin (SYP), NMDAR2A, GABAAR2, calbindin-28K (CALB1), and SNAP25 levels in sFTLD-TDP. GFAP levels showed a

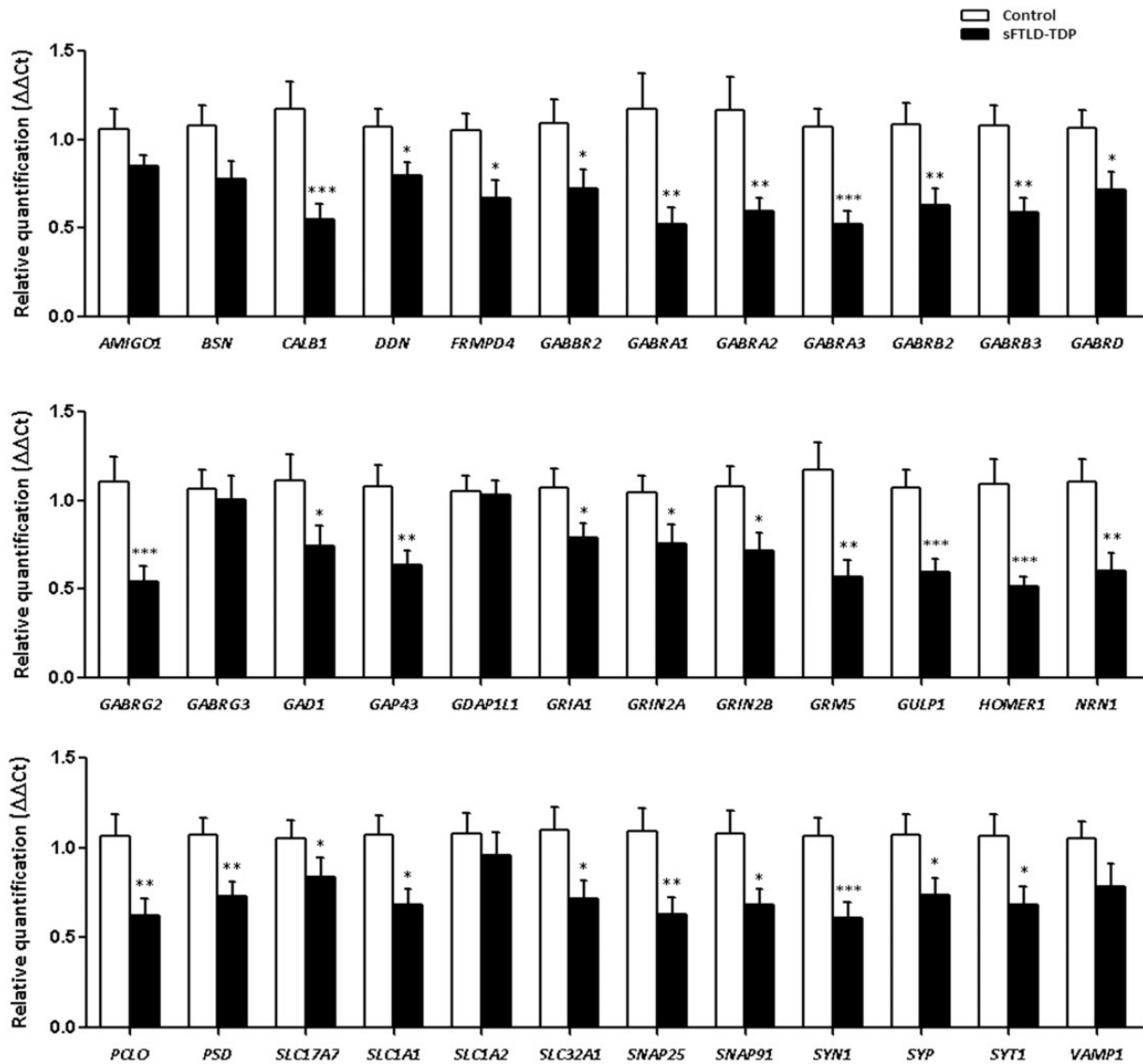


FIGURE 4. mRNA expression levels of selected deregulated genes identified by microarray analysis in frontal cortex area 8 of sFTLD-TDP and controls assessed by TaqMan RT-qPCR assays are coding for glutamatergic and GABAergic-related genes and corresponding ionotropic and metabotropic receptors, as well as synaptic cleft proteins and neurotransmission vesicles system. Significant levels set at * $p < 0.05$, ** $p < 0.01$, and *** $p < 0.001$.

nonsignificant increase in sFTLD-TDP cases when compared with controls (Fig. 6).

revealed with the phospho-tauThr181 antibody was found in sFTLD-TDP (Fig. 7).

Total TAU, 4R-TAU and 3R-TAU

To further analyze cytoskeletal anomalies, the expression levels of total TAU, 3R-TAU, and 4R-TAU were assessed using forward SYBR primer and reverse primer specific probes. Total Tau, 3R-TAU, and 4R-TAU mRNA expression levels were similar in sFTLD-TDP cases when compared with controls. In this line, 4R/3R ratio was preserved in sFTLD cases. Protein expression was studied with Western blotting. Total TAU protein levels were similar in sFTLD-TDP and controls and the ratio 4R/3R was not modified. Finally, no evidence of increased tau phosphorylation, as

Mitochondrial Alterations

Genes Coding for Mitochondrial Subunits and Energy Metabolism

The expression of 37 genes was assessed by RT-qPCR; 27 of them were deregulated in sFTLD-TDP. Downregulated genes encoded subunits of the electron transport chain (ETC) complexes I: *NDUFA2* ($p = 0.02$), *NDUFA5* ($p = 0.05$), *NDUFA10* ($p = 0.016$), *NDUFAF2* ($p = 0.02$), *NDUFAF6* ($p = 0.04$), *NDUFB5* ($p = 0.016$), *NDUFB8* ($p = 0.017$), and *NDUFB10* ($p = 0.025$); subunits of complex IV: *COX7A2L*

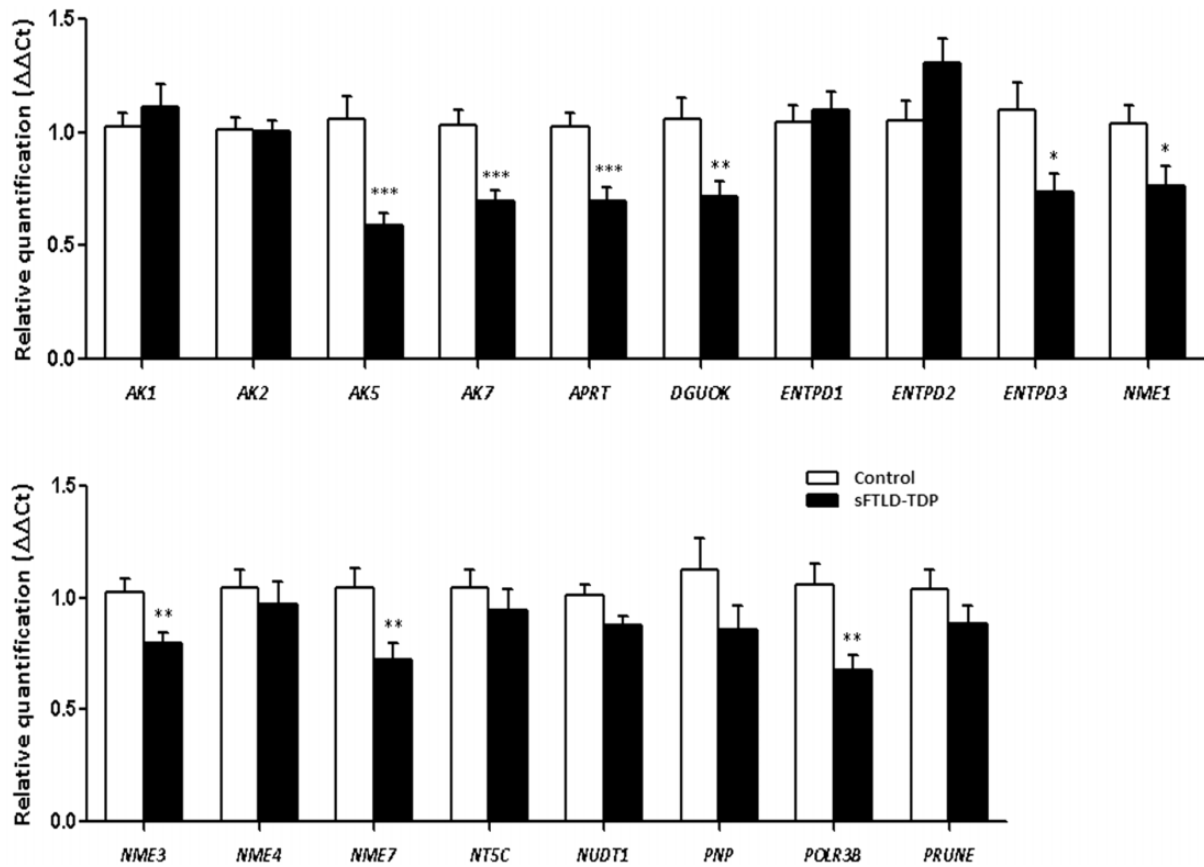


FIGURE 5. mRNA expression levels of selected deregulated genes identified by microarray analysis in frontal cortex area 8 of sFTLD-TDP and controls assessed with TaqMan RT-qPCR assays coding for purines metabolism. Significant levels set at * $p < 0.05$, ** $p < 0.01$, and *** $p < 0.001$.

($p = 0.02$) and *COA6* ($p = 0.02$); and complex V: *ATP5O* ($p = 0.015$), *ATP5A1* ($p = 0.03$), and *ATP5B* ($p = 0.04$). In addition, several genes involved in energy metabolism were downregulated in sFTLD-TDP including *ATP2B3* ($p = 0.03$), *ATP2B4* ($p = 0.04$), *ATP6D* ($p = 0.02$), *ATP6VIA* ($p = 0.002$), *FASTKD2* ($p = 0.007$), *MCU* ($p = 0.045$), *MICU3* ($p = 0.01$), *MTIF2* ($p = 0.006$), *MTX3* ($p = 0.03$), *RMND1* ($p = 0.005$), *SLC25A1* ($p = 0.01$), *SLC25A11* ($p = 0.03$), *SLC25A23* ($p = 0.03$), and *TOMM70* ($p = 0.001$) (Fig. 8A).

Mitochondria Protein Levels in Mitochondria-enriched Fractions

Decreased levels of NDUFB10 were found in sFTLD-TDP ($p = 0.04$), but not of NDUFB8, NDUFS8, NDUFA10. Protein levels of SDHB, a component of ETC complex II, were not modified in sFTLD-TDP. In contrast, UQCRC2, a component of ETC complex III, was significantly increased in sFTLD-TDP ($p = 0.03$). Levels of ATP5A were significantly decreased ($p = 0.04$). MT-CO1 levels were significantly decreased in sFTLD-TDP ($p = 0.01$) but MT-ND1 expression was preserved (Fig. 8B). In contrast to mRNA expression, TOMM70 protein levels were not significantly altered in pathological cases when compared with controls.

Mitochondrial Enzymatic Activities in Mitochondrial Enriched Fractions

The enzymatic activity of mitochondrial complexes I, IV, and V was significantly reduced in sFTLD-TDP cases when compared with controls ($p = 0.04$, $p = 0.03$, and $p = 0.05$, respectively) (Fig. 8C).

DISCUSSION

Gene transcription profiles are analyzed in the frontal cortex area 8 in sFTLD cases with typical neuropathology including TDP-43-immunoreactive inclusions mainly in the form of cortical neurites and intracytoplasmic inclusions. Cases in this series had reduced *TARDBP* mRNA expression and increased levels of TDP-43 protein, and reduced expression of *C9Orf72* mRNA and protein. Opposite expression of TDP mRNA and protein may be related to translational modifications. These are further accompanied by posttranslational modifications of TDP-43 (10). Decreased *C9Orf72* mRNA and protein was not expected and further studies are needed to elucidate *C9Orf72* loss of function in sFTLD-TDP not linked to *C9ORF72* mutations.

The present study using whole-transcriptome microarray hybridization showed downregulation of several genes in

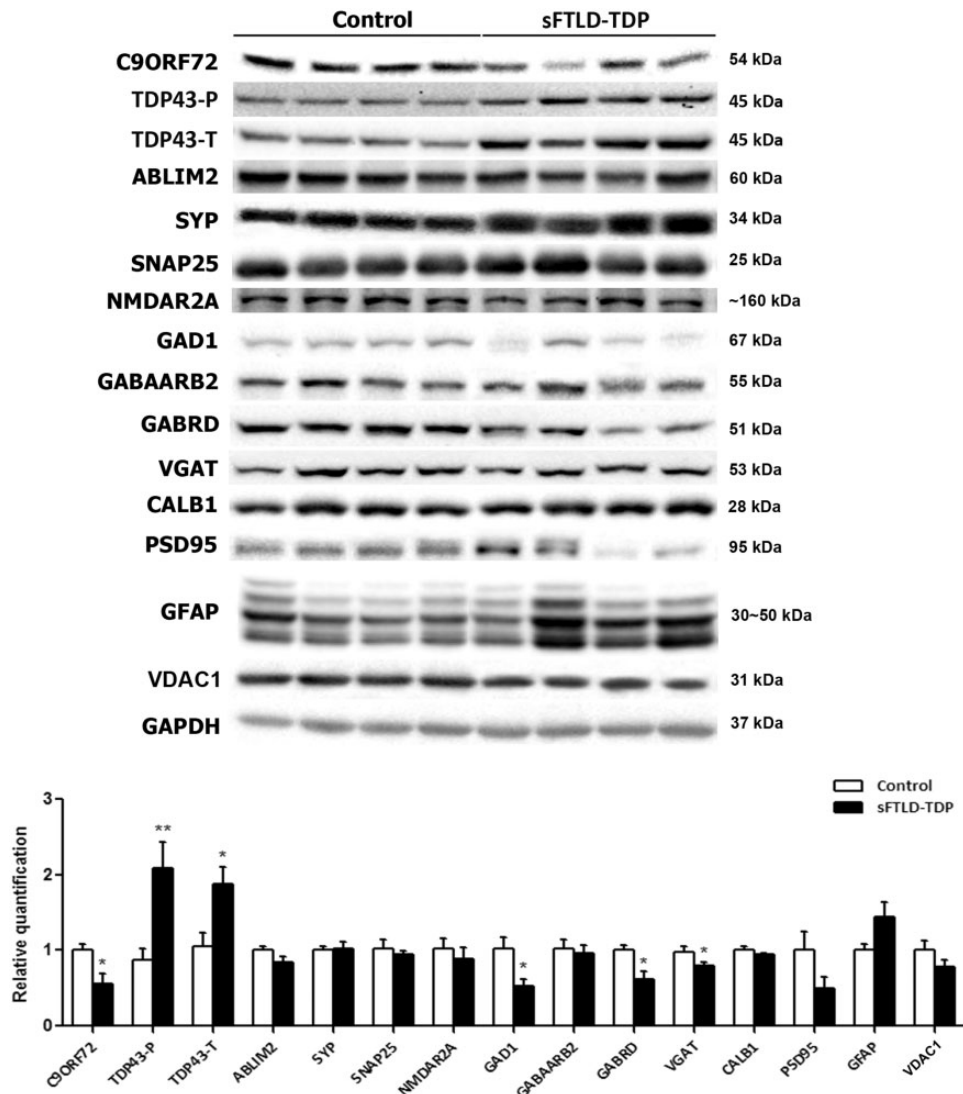


FIGURE 6. Gel electrophoresis and Western blotting of proteins involved in toxic aggregates in FTLD, GABAergic, and glutamatergic neurotransmission systems, synaptic vesicles, cytoskeleton, neuroinflammation, and mitochondria. Significant levels set at * $p < 0.05$, ** $p < 0.01$, and *** $p < 0.001$.

the frontal cortex area 8 in sFTLD-TDP clustered in pathways involved in neurotransmission and synapsis, neuronal architecture, cytoskeleton of axons and dendrites, vesicle trafficking, purine metabolism, mitochondria, and energy metabolism. Microarray observations were further validated by RT-qPCR of selected genes from predicted altered pathways after searching on Gene Ontology (GO) database, using 111 probes; the expression of 81 genes was significantly deregulated in this cortical region in sFTLD-TDP when compared with controls. Expression levels of 24 proteins were analyzed by Western blotting; levels of 8 proteins were altered in sFTLD-TDP. Neurotransmission was markedly affected in sFTLD-TDP involving downregulated gene expression of glutamate decarboxylase, several types and subunits of ionotropic and metabotropic glutamate and GABA receptors, neuronal vesicular and soluble glutamate transporters, and various

synaptic proteins, together with loss of calbindin expression. This provides robust support to preliminary observations showing decreased numbers, amputation, and proximal swellings of dendritic branches and loss of synaptic spine pyramidal cells, and loss of calbindin-immunoreactive neurons and atrophy of remaining neurons in layers II and III of the frontal cortex in FTLD (24). Protein expression studies showing decreased levels of synaptic markers are also in line with previous observations demonstrating reduced levels of several synaptic and presynaptic plasma membrane proteins in the frontal cortex, but not in the posterior parietal cortex assessed in parallel, in FTLD (25).

In contrast to the marked decrease in the expression of cytoskeletal and synaptic markers, tau mRNA and protein levels were preserved in the present series, and tau phosphorylation was not increased in sFTLD-TDP. This is in contrast with

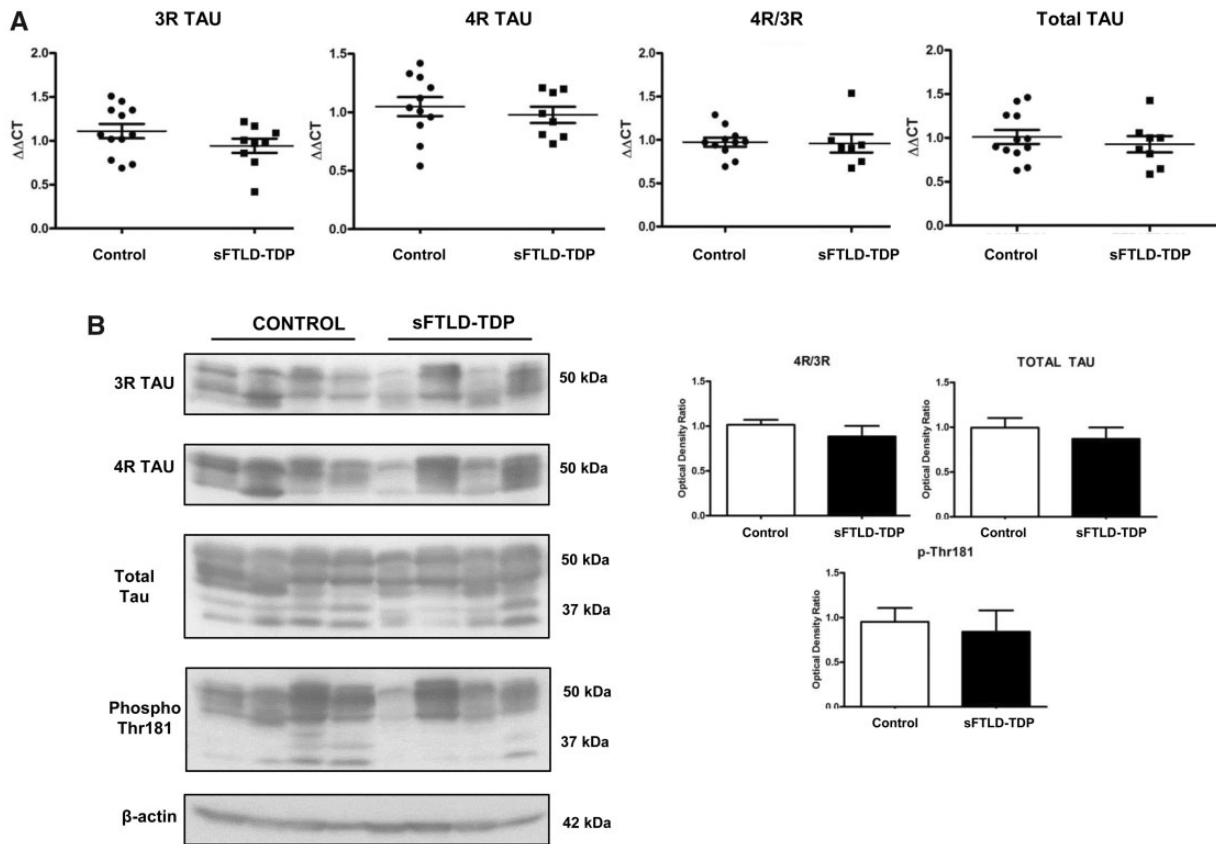


FIGURE 7. (A) mRNA expression levels of total TAU, 3R-TAU, and 4R-TAU in the frontal cortex area 8 in control and sFTLD-TDP. No significant differences are observed and the ratio 4R/3R is similar in sFTLD and controls. **(B)** Similarly, no differences in TAU protein expression and 4R/3R are seen in sFTLD-TDP cases and controls. Phospho-tau levels, as revealed with the phospho-tau-specific Thr181 antibody, are similar in control and sFTLD-TDP.

early reports pointing to decreased tau protein levels in FTLT with ubiquitin inclusions (presumably FTLT-TDP), which suggested that FTLT-U may be a novel “inverse” tauopathy because of the reduced levels of tau (26, 27). Reduced tau mRNA and protein levels have been reported in FTLT-TDP linked to GRN mutations but not in other FTLT-TDP subtypes including sporadic FTLT-TDP and FTLT-TDP-C9ORF72 (28).

Mitochondrial alterations compromise mRNA expression of several subunits of the mitochondrial complexes. Moreover, they are accompanied by altered protein expression of several subunits and with reduced activity of complexes I, IV, and V in sFTLD-TDP. Importantly, in addition to mitochondrial subunits encoded by genomic DNA, expression levels of MT-CO1 encoded by mitochondrial DNA are reduced in sFTLD-TDP. Therefore, mitochondrial alterations in sFTLD-TDP have both genomic and mitochondrial components. Other genes involved in energy metabolism are downregulated as well, thus indicating functional energy metabolism failure in sFTLD-TDP. Gene-specific mitochondrial dysfunction has been described in human fibroblasts bearing mutations in *TARDBP* and *C9ORF72* (29). Mitochondrial dysfunction has also been documented in a transgenic knock-in

mouse model for TDP-43 (30). Therefore, mitochondrial alterations seem to be common to different forms of sFTLD-TDP and fFTLD-TDP.

Purines and pyrimidines are components of a large number of key molecules. The primary purines adenine and guanine, and pyrimidines cytosine, thymidine, and uracil, are the core of DNA, RNA, nucleosides, and nucleotides involved in energy transfer (ATP, GTP) and coenzymes (NADH, FADH2) (31, 32). Alterations in the expression of genes encoding enzymes of purine metabolism may interfere with numerous metabolic processes in sFTLD-TDP.

It can be argued that differences in the percentage of neurons, astrocytes, oligodendroglia, and microglia lie beyond distinct patterns of gene expression, protein levels, and mitochondrial enzymatic activities in sFTLD-TDP. Certainly, neuron loss, spongiosis in the upper cortical layers and variable astrocytic gliosis are typical morphological alterations in sFTLD-TDP (1–3). Present findings complement morphological observations by biochemical data that identify damage of particular components of vital molecular pathways and essential modulators of synaptic transmission.

Previous studies have shown differential gene expression in frontal cortex between 6 cases of FTLT-U

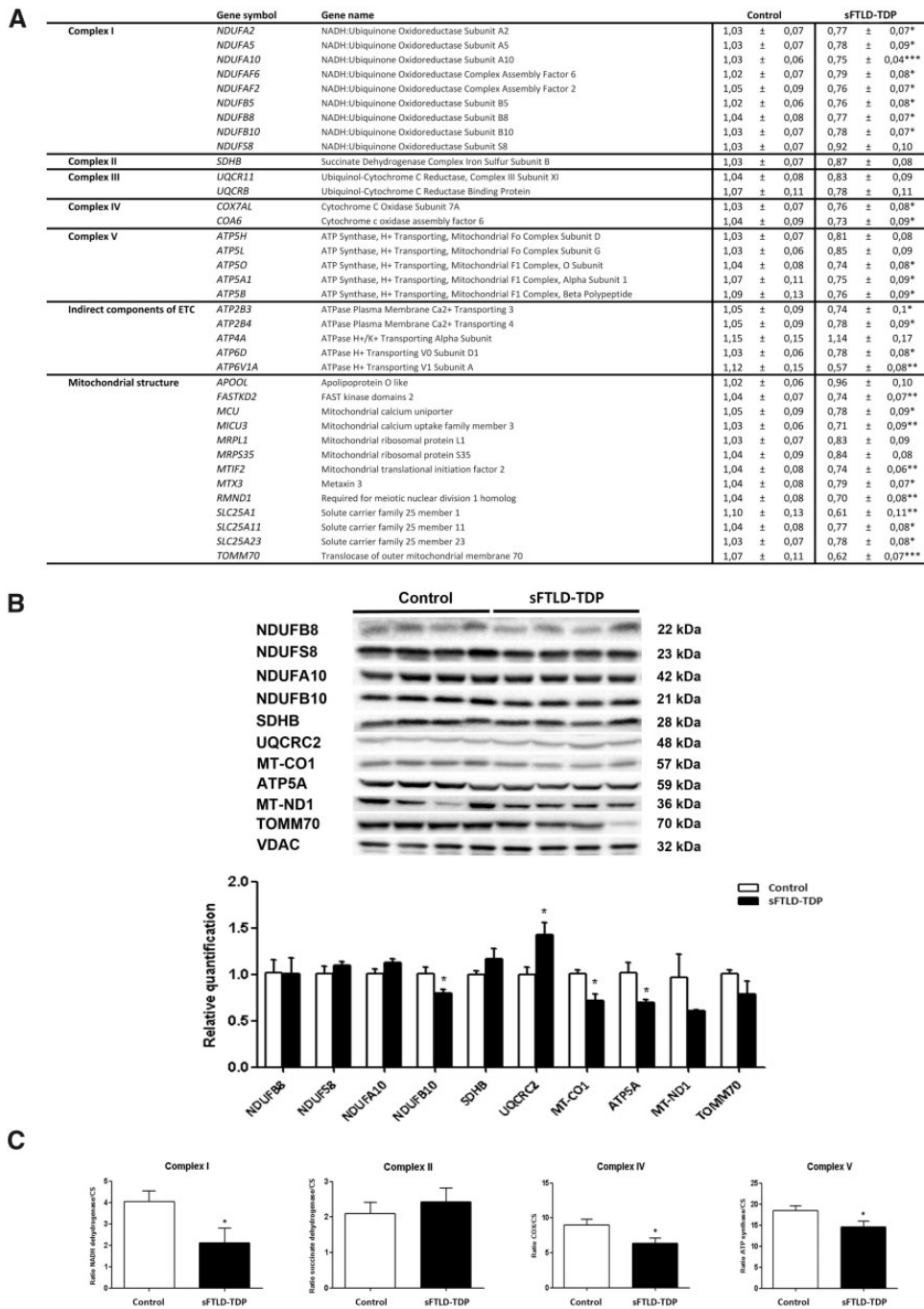


FIGURE 8. (A) mRNA expression levels of selected deregulated genes identified by microarray analysis in the frontal cortex area 8 of sFTLD-TDP and controls assessed with TaqMan RT-qPCR assays coding for subunits of the mitochondrial respiratory chain and proteins linked to energy metabolism. **(B)** Protein levels in control and sFTLD-TDP of subunits encoded by genomic DNA of mitochondrial complexes I (NDUFA10, NDUFB10, NDUFS8, NDUFB8), II (SDHB), III (UQCRC2), and V (ATP5A); encoded by mitochondrial DNA of complex I (MT-ND1) and complex IV (MTCO1); and TOMM10 normalized with voltage-dependent anion channel (VDAC). Diagrams show quantitative values of all assessed cases. **(C)** Mitochondrial enzymatic activities in complex I, II, IV, and V in control and FTLD. All the mitochondrial activities are corrected with citrate synthase activity. Significant levels set at * $p < 0.05$, ** $p < 0.01$, and *** $p < 0.001$.

(FTLD-TDP), 3 of them bearing *GRN* mutations, and 4 FTLD-MND (linked to motor neuron disease) cases. RT-qPCR validated the deregulation of dynein, annexinA2, and

myeloid differentiation primary response in FTLD-U (14). Another study examined 7 FTLD-U cases linked to *GRN* mutations and 10 FTLD-U cases without *GRN* mutations (15).

A distinct molecular phenotype was identified for *GRN*+FTLD-U when compared with *GRN*-FTLD-U subtypes. Validation by RT-qPCR was assessed for 16 genes; deregulated biological processes associated with *GRN*-FTLD-U were lipid metabolism, MAPK signaling pathways, and transport (15). A recent study in the cerebellum and frontal cortex in sALS and ALS linked to *C9ORF72* mutations has shown 57 genes in cerebellum and 32 genes in frontal cortex abnormally expressed in both c9ALS and sALS; however, the number of deregulated genes in *C9ORF72* sALS cases was double than in sALS thus further suggesting differences between different forms of ALS (19).

Comparison between present findings and our previous observations in frontal cortex area 8 in sALS (18), using the same methods, is worth stressing since most of downregulated genes in sFTLD-TDP are upregulated in the frontal cortex area 8 in sALS cases without dementia (18). This suggests a primary response to synaptic and neurotransmission disturbances of frontal cortex area 8 at preclinical stages of frontal degeneration in sALS. Reduced expression of genes encoding actin, actin-related members, kinesin, and microtubule-associated protein further supports cytoskeletal damage in sALS and sFTLD-TDP.

Conclusions

Whole transcriptome arrays and bioinformatics processing followed by RT-qPCR expression of 111 genes shows deregulation of 81 genes involved in cytoskeleton and neuron structure, neurotransmitters, receptors, transporters and synaptic proteins, components of mitochondrial function and energy metabolism, enzymes involved in purine metabolism and RNA splicing in sFTLD-TDP. Western blotting of selected proteins further supports alterations of these pathways at translational level. Finally, altered mitochondrial activity of several mitochondrial complexes is demonstrated by enzymatic assays.

ACKNOWLEDGMENTS

We are indebted to the Neurological Tissue Bank of the IDIBAPS Biobank, Barcelona, Spain, for sample and data procurement. Microarrays were carried out at the High Technology Unit (UAT), Vall d'Hebron Research Institute (VHIR), Barcelona, Spain. We wish to thank F. Briansó, Unit of Statistics and Bioinformatics, VHIR, for the preliminary bioinformatics processing of data, and T. Yohannan for editorial help.

REFERENCES

- Hortobagyi T, Cairns NJ, Amyotrophic lateral sclerosis and frontotemporal lobar degeneration. In: Kovacs Gabor G, eds. *Neuropathology of Neurodegenerative Diseases: A Practical Guide*. Cambridge: Cambridge University Press 2015:209–48
- Lashley T, Roher JD, Mead S, et al. Review: an update on clinical, genetic and pathological aspects of frontotemporal lobar degenerations. *Neuropathol Appl Neurobiol* 2015;41:858–81
- Mann DMA, Snowden JS. Frontotemporal lobar degeneration: pathogenesis, pathology and pathways to phenotype. *Brain Pathol* 2017;27:723–36
- Olszewska DA, Lonergan R, Fallon EM, et al. Genetics of frontotemporal dementia. *Curr Neurol Neurosci Rep* 2016;16:107
- Pottier C, Ravenscroft TA, Sanchez-Contreras M, et al. Genetics of FTL: Overview and what else we can expect from genetic studies. *J Neurochem* 2016;138:32–53
- Rainero I, Rubino E, Michelero A, et al. Recent advances in the molecular genetics of frontotemporal lobar degeneration. *Funct Neurol* 2017;32:7–16
- Geser F, Martinez-Lage M, Robinson J, et al. Clinical and pathological continuum of multisystem TDP-43 proteinopathies. *Arch Neurol* 2009;66:180–9
- Cruts M, Gijselink I, Van Langenhove T, et al. Current insights into the *C9orf72* repeat expansion diseases of the FTL/ALS spectrum. *Trends Neurosci* 2013;36:450–99
- Renton AE, Chiò A, Traynor BJ. State of play in amyotrophic lateral sclerosis genetics. *Nat Neurosci* 2014;17:17–23
- Neumann M, Sampathu DM, Kwong LK, et al. Ubiquitinated TDP-43 in frontotemporal lobar degeneration and amyotrophic lateral sclerosis. *Science* 2006;314:130–3
- Mackenzie IR, Neumann M, Baborie A, et al. A harmonized classification system for FTL-TDP pathology. *Acta Neuropathol* 2011;122:111–3
- Alafuzoff I, Pikkarainen M, Neumann M, et al. Neuropathological assessments of the pathology in frontotemporal lobar degeneration with TDP43-positive inclusions: An inter-laboratory study by the BrainNet Europe consortium. *J Neural Transm (Vienna)* 2015;122:957–72
- Mackenzie IR, Neumann M. Molecular neuropathology of frontotemporal dementia: Insights into disease mechanisms from postmortem studies. *J Neurochem* 2016;138:54–70
- Mishra M, Paunesku T, Woloschak GE, et al. Gene expression analysis of frontotemporal lobar degeneration of the motor neuron disease type with ubiquitinated inclusions. *Acta Neuropathol* 2007;114:81–94
- Chen-Plotkin AS, Geser F, Plotkin JB, et al. Variations in the progranulin gene affect global gene expression in frontotemporal lobar degeneration. *Hum Mol Genet* 2008;17:1349–62
- Martins-de-Souza D, Guest PC, Mann DM, et al. Proteomic analysis identifies dysfunction in cellular transport, energy, and protein metabolism in different brain regions of atypical frontotemporal lobar degeneration. *J Proteome Res* 2012;11:2533–43
- Evers BM, Rodriguez-Navas C, Tesla RJ, et al. Lipidomic and transcriptomic basis of lysosomal dysfunction in progranulin deficiency. *Cell Rep* 2017;20:2565–74
- Andrés-Benito P, Moreno J, Aso E, et al. Amyotrophic lateral sclerosis, gene deregulation in the anterior horn of the spinal cord and frontal cortex area 8: Implications in frontotemporal lobar degeneration. *Aging* 2017;9:823–51
- Prudencio M, Belzil VV, Batra R, et al. Distinct brain transcriptome profiles in *C9orf72*-associated and sporadic ALS. *Nat Neurosci* 2015;8:251175–82
- Ferrer I, Martinez A, Boluda S, et al. Brain banks: Benefits, limitations and cautions concerning the use of post-mortem brain tissue for molecular studies. *Cell Tissue Bank* 2008;9:181–94
- van der Zee J, Gijselink I, Dillen L, et al. A pan-European study of the *C9orf72* repeat associated with FTL: Geographic prevalence, genomic instability, and intermediate repeats. *Hum Mutat* 2013;34:363–73
- Gentleman RC, Carey VJ, Bates DM, et al. Bioconductor: Open software development for computational biology and bioinformatics. *Genome Biol* 2004;5:R80
- Barrachina M, Castaño E, Ferrer I. TaqMan PCR assay in the control of RNA normalization in human post-mortem brain tissue. *Neurochem Int* 2006;49:276–84
- Ferrer I. Dementia of frontal lobe type and amyotrophy. *Behav Neurol* 1992;5:87–96
- Ferrer I. Neurons and their dendrites in frontotemporal dementia. *Dement Geriatr Cogn Disord* 1999;10(Suppl 1):55–60
- Zhukareva V, Sundarraj S, Mann D, et al. Selective reduction of soluble tau proteins in sporadic and familial frontotemporal dementias: An international follow-up study. *Acta Neuropathol* 2003;105:469–76
- Zhukareva V, Vogelsberg-Ragaglia V, Van Deerlin VM, et al. Loss of brain tau defines novel sporadic and familial tauopathies with frontotemporal dementia. *Ann Neurol* 2001;49:165–75
- Papegacy A, Eddarkaoui S, Deramecourt V, et al. Reduced Tau protein expression is associated with frontotemporal degeneration with progranulin mutation. *Acta Neuropathol Commun* 2016;4:74

29. Onesto E, Colombrina C, Gumina V, et al. Gene-specific mitochondria dysfunctions in human TARDP and C9ORF72 fibroblasts. *Acta Neuropathol Commun* 2016;4:47
30. Stribl C, Samara A, Trümbach D, et al. Mitochondrial dysfunction and decrease in body weight of a transgenic knock-in mouse model for TDP-43. *J Biol Chem* 2014;289:10769–84
31. Ipata PL, Camici M, Micheli V, et al. Metabolic network of nucleosides in the brain. *Curr Top Med Chem* 2011;11:902–22
32. Ansoleaga B, Jové M, Schlüter A, et al. Deregulation of purine metabolism in Alzheimer's disease. *Neurobiol Aging* 2015;36:68–80